NASA CONTRACTOR REPORT

NASA CR-633

NASA CR-633

THE INTERNAL COMPTON EFFECT

by M. P. Bedesem and K. J. Casper

Prepared by
WESTERN RESERVE UNIVERSITY
Cleveland, Ohio
for

NATIONAL AERONAUTICS AND SPACE ADMINISTRATION • WASHINGTON, D. C. • NOVEMBER 1966

NASA CR-633

THE INTERNAL COMPTON EFFECT

By M. P. Bedesem and K. J. Casper

Prepared under Grant No. NsG-655 by
WESTERN RESERVE UNIVERSITY
Cleveland, Ohio

for

NATIONAL AERONAUTICS AND SPACE ADMINISTRATION

For sale by the Clearinghouse for Federal Scientific and Technical Information
Springfield, Virginia 22151 – Price $2.50

TABLE OF CONTENTS

	Page
LIST OF TABLES	iv
LIST OF ILLUSTRATIONS	v
Chapter	
I. INTRODUCTION	1
II. THEORY	4
A. Cooper and Morrison	4
B. Knipp and Uhlenbeck	6
C. Chang and Falkoff	8
D. Baumann and Robl	8
E. Iakobson	10
F. Spruch and Goertzel	12
G. L Shell Internal Compton Effect Coefficients	13
III. APPARATUS-SUPERCONDUCTING MAGNET SPECTROMETER	16
A. Description of Equipment	17
B. Operation and Experiments	27
C. Conclusion	34
IV. ANALYSIS	35
V. CONCLUSION	53
LIST OF REFERENCES	57

LIST OF TABLES

Table		Page
I.	Comparison of K/L Ratios	38
II.	Comparison of Intensity ratios	38
III.	Multipolarity Predictions for α_K Known	51
IV.	Multipolarity predictions for α_K From Born approximation	51
V.	Character and Multipolarity Predictions	52

LIST OF ILLUSTRATIONS

Figure		Page
1.	Idealized electron and gamma ray distributions of the internal Compton effect.	5
2.	Superconducting magnet spectrometer.	18
3.	Arrangement of detector probe in solenoid.	19
4.	Magnetic field intensity along axis of solenoid.	22
5.	Maximum electron radius for a particle emitted perpendicular to the magnetic field B.	24
6.	Assumptions for calculating the fraction of the electrons emitted within an angle ϕ.	25
7.	The percentage of the emitted particles not collected within the integration time of the amplifier	28
8.	Block diagram of the electronics used with the superconducting magnet spectrometer.	29
9.	Data taken with one detector, with and without the field.	31
10.	Data taken with the magnetic field and two detectors in parallel.	32
11.	Comparison of the background spectra to the data	33
12.	Internal conversion line shape determined by folding over the high energy side of the peak.	36
13.	The effect of detector resolution on an idealized conversion line and a continuous distribution.	39
14.	Comparison of the K shell theoretical calculations for the internal Compton effect with the data.	42
15.	Comparison of the L shell theoretical calculations for the internal Compton effect with the data.	45

Figure Page

16. Comparison of the K + L shell theoretical calculations for the internal Compton effect with the data. 46

17. Multipolarity dependence of Baumann and Robl's calculation where the internal conversion coefficient is known 48

18. Multipolarity dependence of Baumann and Robl's calculation where the internal conversion coefficient is taken from calculations in the Born approximation . . 49

19. The Z dependence of the internal Compton effect coefficient. 55

CHAPTER I

INTRODUCTION

The decay of a nucleus in an excited state is usually considered as proceeding by the independent processes of gamma ray emission and internal conversion, which, when detected, yield monoenergetic distributions in energy. However, it has been observed that the conversion electron spectrum of various nuclear decays contains a continuous distribution of electrons in the energy range just below the K shell conversion line. The presence of this continuous distribution has been ascribed to the internal Compton effect in which an orbital electron and a gamma ray are simultaneously emitted and share the energy of the nuclear transition. In analogy to the external Compton effect, the process can be considered to take place by means of the nucleus emitting a virtual gamma ray which scatters off the atomic electrons and results in an ionized electron and a real gamma ray being emitted. As in internal conversion, the virtual gamma ray is the field characterized by the periodic oscillations of the electric or magnetic moment of the nuclear charge distribution. Taylor and Mott[1] have shown that the process where the atomic electrons de-excite the nucleus proceeds by direct interaction of the inner electrons with the nucleus, and that it is not a phenomenon uniquely involving a real gamma ray in the initial state. The nomenclature of internal Compton effect is a result of the interpretation in which the nuclear field is characterized as a

virtual gamma ray. In this case, the interaction can be described as a scattering process similar to that of the external Compton effect with the exception that the initial photon is no longer a plane wave.

Internal bremsstrahlung, a process resulting in the same final states of electron and gamma ray, is described as the radiation accompanying charged particle transformation in processes like beta decay. Classically, it is also possible to think of the internal Compton effect as being of a bremsstrahlung origin if one considers the radiation to occur when the inner shell electrons interact with the nuclear field and are accelerated to an ionized state. Under these conditions, the internal Compton effect could be described as radiative conversion[2] resulting from the emission of a photon in the internal conversion process.

The internal Compton effect, in comparison to other nuclear processes, is quite small. Its intensity is less than that of the conversion by a factor the order of α, the fine structure constant, and less than gamma ray emission by a factor of α^2. The observation of the internal Compton effect can easily be obscured by the presence of background radiation resulting from the Compton scattering of higher energy gamma rays in the source or detector, from a backscattering distribution of the conversion line, or by a competing beta decay. Because these experimental problems have made direct observation of the electron spectrum of the internal Compton effect very difficult, experimenters have instead considered the angular correlation between the electron and the scattered gamma ray.[3,4,5,6]

In performing this experiment we sought to confirm the existence of the internal Compton effect and to investigate whether the distributions

could be used to determine the multipolarity of nuclear transitions.

At present, multipolarity assignments are made on the basis of angular correlation experiments or by comparing the internal conversion coefficients with the theoretical predictions. Because of persistent problems with efficiency and solid angle ratios, statistics, scattering, and background, the above methods sometimes yield ambiguous results.

Determining the multipolarity assignments by observing the internal Compton effect with the superconducting magnet spectrometer has several possible advantages. The design of the spectrometer has eliminated all instrumental distortions from the electron spectrum and enables small effects to be observed without coincidence techniques. By fitting the theoretical distributions for the internal Compton effect to the data there are two criteria on which to judge the multipolarity assignment: the intensity of the effect as a function of multipole order, and the shape of the energy distribution as a function of multipolarity. Either or both of these criteria, in conjunction with the theoretical calculations for the internal conversion coefficients, may be able to lead to a new method of determining the multipolarity of a converted nuclear decay.

CHAPTER II

THEORY

The first consideration of the internal Compton effect was made by E. P. Cooper and P. Morrison[7] who termed the process the internal scattering of gamma rays. Several experimenters[8] had noted that the spectrum of ThC" contained an unexpectedly large number of electrons in the energy range just below the strong K shell conversion line from a 2.62 MeV transition. It was realized that these electrons appeared above the upper limit for the energy that a recoil electron could receive in Compton scattering in the source. In Compton scattering, the incident quantum cannot transmit an arbitrary amount of its energy to the electron because of the conservation of momentum between the incident plane wave and the free electron. In the internal Compton effect, however, the electron interacts with the spherical multipole field of the nucleus, which being a heavy body, can take up momentum without removing a significant amount of energy. This relaxes the momentum requirements on the gamma quantum and allows the electron to acquire any energy up to the energy of the transition minus the binding energy.

An idealized sketch of the internal Compton effect showing the electron and gamma distributions is given in Figure 1. For any event, the sum of the scattered electron energy, E_e, and the photon energy, k,

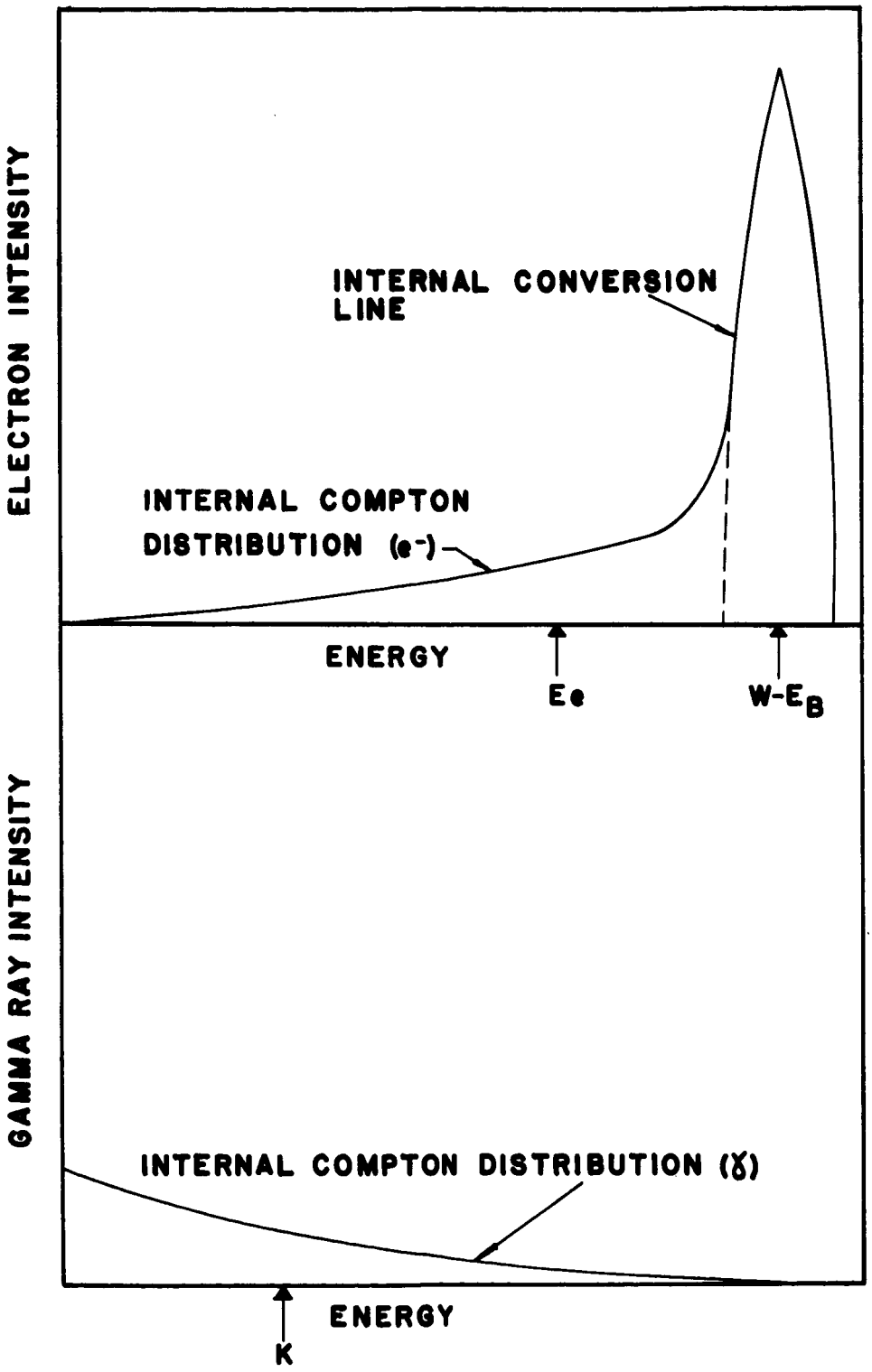

Fig. 1 Idealized electron and gamma ray distributions of the internal Compton effect. The arrows indicate one set of energies satisfying the relationship $E_e + k = W - E_B$.

must be equal to the energy of the transition minus the binding energy.

$$E_e + k = W - E_B = W' \qquad (1)$$

Cooper and Morrison limited their calculation to consideration of scattering of the s electrons from the K shell by a quantized electric dipole radiation field in the limit that the transition energy approaches infinity. This restriction is not easily applied to transitions of 1 MeV or less, so this calculation is not included for comparison with the data. It is interesting to note, however, that at the time the calculation was performed, the result was so small that Cooper and Morrison reached the conclusion that the spectrum was instrumentally produced.

The calculations which we will compare with the observed data can be subdivided into two classes: those which describe the probability of a K shell electron interacting with the nuclear field and subsequently ejected with a photon, and those which describe the process as bremsstrahlung of the emitted conversion electrons.

The internal bremsstrahlung of charged particles was derived by Knipp and Uhlenbeck[9] to explain the continuous radiation which accompanies beta decay. The process, as applied to internal conversion, is interpreted as the radiation emitted as an electron is leaving the field of the nucleus with a definite energy. They have calculated, using relativistic quantum mechanics and the Born approximation for the final electron state, the probability that an electron, born at the nucleus at a time t = 0 with an energy W', will emit a quantum of energy k. To find the probability that the system of the electron and

the radiation field be in the final state with a total energy $W' = E_e + k$ at a time t, first order perturbation theory for a one photon change was employed. The initial electronic wave functions were free, outgoing, nonallowed solutions to the Dirac equation and were necessary to describe an electron leaving the nucleus and to give rise to radiation. The result of the calculation for an allowed transition of the nucleus is

$$d\phi = \frac{\alpha p \sin\theta d\theta}{2\pi p_e k}\left[\frac{W^2 + E_e^2}{W(E_e - p\cos\theta)} - \frac{1}{(W - p\cos\theta)^2} - 1\right] \quad (2)$$

or by integrating over θ,

$$\phi = \frac{\alpha p}{\pi p_e k}\left[\frac{W^2 + E_e^2}{Wp} \log (E_e + p) - 2\right] \quad (3)$$

where θ is the angle between the observed electron and gamma ray of momentum p and k respectively, α is the fine structure constant, and W and p_e are the energy and momentum of the electron as it is created. Throughout this paper we will use the system of units where $\hbar = c = m = 1$. Equations (2) and (3) express the differential and total probability per unit time than an electron, already created and leaving the nucleus, will radiate a quantum of energy k and itself be detected with an energy E_e. When applied to the process of internal conversion, the total probability function is interpreted as the quotient of the probability per unit time for the internal Compton effect and the probability per unit time for the conversion process. This relative probability, ϕ, is then called the internal Compton coefficient. The calculations are expected to be valid for low Z and particle of high energy as required by the Born approximation ($Z\alpha/p \ll 1$). The probabilities are independent of Z and multipole order which restricts their

applicability and expected accuracy for predicting the internal Compton effect in most nuclei.

C. S. W. Chang and D. L. Falkoff[10] have developed a similar expression for the probability of electron bremsstralung from semi-classical methods. Their calculation is based on the classical assumption that an accelerated charge radiates, and in this case they have assumed that the electron leaving the nucleus was given its velocity instantaneously at t = 0. Here Z is set equal to zero and no attempt is made to account for the manner in which the electron received its energy. The result of this derivation yields

$$d\phi = \frac{\alpha}{2\pi k} \frac{\beta^2 \sin^2\theta \sin\theta d\theta}{(1 - \beta\cos\theta)^3} \tag{4}$$

where $\alpha = 1/137$ and $\beta = v/c$. By integrating over θ, one gets

$$\phi = \frac{\alpha}{\pi k} \left[\frac{1}{\beta} \ln \frac{1 + \beta}{1 - \beta} - 2 \right] \tag{5}$$

This is the same result that can be arrived at from the Knipp-Uhlenbeck theory if one makes the substitutions $W = E_e$, $p_e = p$ required by the assumption that k is small, and $p/E_e = \beta$, $W^2 = 1/(1 - \beta^2)$ derived from the relativistic electron relationships. In both cases, in order to arrive at numerical results for the internal Compton effect, it is necessary to multiply by the number of internal conversion electrons emitted.

Baumann and Robl[11] have calculated an exact quantum mechanical extention of the work done by Chang and Falkoff on internal bremsstrahlung. They calculate the probability for emission of an electron and a coincident

gamma ray under the condition k>>Z/137 which requires that the observed gamma ray be of high energy and the nucleus be of small atomic number. Their calculation, limited to interactions with the K shell electrons, and performed with relativistic wave functions, yields the following result for the electric and magnetic transitions of multipole order ℓ.

$$d\Psi_{ele} = \eta \frac{\ell}{\ell+1}\left[\frac{1}{K}\frac{p^2\sin^2\theta}{(E_e - p\cos\theta)^2}\left[E_e + 1 - 2\lambda p\sigma_K + \lambda^2\frac{2\ell+1}{\ell}(E_e - 1)\right] + \frac{1}{(E_e - p\cos\theta)^2}\right.$$

$$\left[-1 + 2\lambda\sigma_p - \lambda^2\frac{2\ell+1}{\ell}\right] + \frac{1}{E_e - p\cos\theta}\left[2E_e - 1 - K + 2\lambda\left[(E_e^2 - E_e + K)\sigma_p - p\sigma_K\right] + \lambda^2\left[2p^2\right.\right.$$

$$-2K - 2E_e p\cos\theta + \frac{2\ell+1}{\ell}(2E_e + 1 + K) + K\left(\frac{\ell-1}{\ell}\right)\left(\frac{p}{q}\right)^2(1 - E_e - K)\sin^2\theta\Big]\Big] + (1+K)(E_e +$$

$$p\cos\theta) - 1 - 2\lambda\left[E_e(1+K)\sigma_p + pK\sigma_K\right] + \lambda^2\left[(1+K)\left[2p\cos\theta + \left(\frac{\ell-1}{\ell}\right)K\left(\frac{p}{q}\right)^2\sin^2\theta\right] + \frac{2\ell+1}{\ell}\right.$$

$$\left.\left.\left[(1+K)(E_e - p\cos\theta) - (2E_e + 1)\right]\right]\right]\sin\theta\, d\theta\, dK \qquad (6)$$

$$d\Psi_{mag} = \eta\left[\frac{1}{(E_e - p\cos\theta)^2}\left[\frac{1}{K}(W - K)p^2\sin^2\theta - 1\right] + \frac{1}{E_e - p\cos\theta}\left[2E_e + 1 - K + KW\left(\frac{p}{q}\right)^2\sin^2\theta\right]\right.$$

$$\left.-(2E_e + 1) + (1+K)(E_e - p\cos\theta) - K(1+K)\left(\frac{p}{q}\right)^2\sin^2\theta\right]\sin\theta\, d\theta\, dK \qquad (7)$$

where

$$\eta = \frac{2\alpha^2}{\pi}(Z\alpha)^3\frac{p}{W}\left(\frac{q}{W}\right)^{2\ell}\frac{1}{(q^2 - W^2)^2 + 2(Z\alpha)^2(q^2 + W^2) + (Z\alpha)^4}$$

$$\lambda = \frac{W}{q}\ ,\quad \sigma_p = \left[1 - \left(\frac{p}{q}\right)^2\sin^2\theta\right]^{1/2}\ ,\quad \sigma_K = \left[1 - \left(\frac{K}{q}\right)^2\sin^2\theta\right]^{1/2}$$

where $\vec{q} = \vec{p} + \vec{k}$, W equals the transition energy, E and p are the final energy and momentum of the electron, k is the energy of the gamma ray, and θ the angle between the electron and the gamma ray. In these calculations $d\psi$ represents the differential probability per unit time for the internal Compton effect divided by the probability per unit time that the nucleus undergoes a transition. To calculate the electron spectrum versus the energy of the electron, it is necessary to numerically integrate these equations over θ, the direction of the gamma ray, and multiply by the total number of transitions.

In the limiting case where $k \to 0$, or $q \to p$, the Baumann-Robl theory reduces to the semi-classical result of Chang and Falkoff for bremsstrahlung for small energy losses.

A. M. Iakobson[12] has developed a nonrelativistic perturbation approach under the restriction that the transition energy be much less than the electron rest energy. The calculation assumes a nonrelativistic interaction between a charged particle and the electromagnetic field which he quantizes with spherical waves. Hydrogen-like, nonrelativistic wave functions were used for the electron and the final state treated in the Born approximation where only the long wavelength part of the gamma spectrum was considered. The internal Compton effect is calculated as a relative probability coefficient defined as the ratio of the probability of the internal Compton effect to the probability for the nucleus to emit a gamma ray from the same transition. The results for the electric and magnetic multipole transitions are

$$\chi \text{ magnetic} = \frac{8}{3\pi} \left(\frac{\ell}{\ell + 1} \right) \alpha^2 \, (Z\alpha)^3 \left[\frac{2}{W} \right]^{\ell + 3/2} \cdot \frac{dk}{k} \tag{8}$$

$$\chi \text{ electric} = \frac{8}{3\pi} \, \alpha^2 \, (Z\alpha)^3 \left[\frac{2}{W} \right]^{\ell + 1/2} \frac{dk}{k} \tag{9}$$

Iakobson also includes the results of dividing his relative probability coefficient, χ, by the expression for the internal conversion coefficient for the same character transition. This relative probability, termed the internal Compton coefficient, the same for both the electric and magnetic transitions, is now independent of multipolarity and Z.

$$\phi = \frac{\chi \text{ Ele}}{\alpha_K^{\text{Ele}}} = \frac{\chi \text{ Mag}}{\alpha_K^{\text{Mag}}} = \left[\frac{4\alpha}{3\pi}\right] \frac{1}{W} \frac{dk}{k} \qquad (10)$$

The angular dependence between the electron and gamma ray has been integrated out in both sets of equations and therefore this calculation is not suited to angular correlations.

Equation (10) induced Iakobson to suggest that perhaps the probability of the internal Compton effect is equal to the product of the probability for internal conversion and the probability that the electron emits as it leaves the atom. We can compare this with Chang and Falkoff's result by expanding their expression for the internal Compton coefficient as follows.

$$\phi = \frac{\alpha}{\pi k} \left[\frac{1}{\beta} \ln \left(\frac{1+\beta}{1-\beta}\right) - 2\right]$$

and since

$$\ln \left(\frac{1+\beta}{1-\beta}\right) \doteq 2 \left[\beta + \frac{\beta^3}{3} + \frac{\beta^5}{5} + \cdots\right]$$

$$0 \doteq \frac{\alpha}{\pi k} \left[\frac{1}{\beta}\left(2\beta + \frac{2\beta^3}{3}\right) - 2\right] = \frac{2\alpha}{3\pi} \left[\beta^2\right] \frac{1}{k}$$

where

$$\beta = p/E_e, \; m = 1$$

therefore

$$\phi = \frac{2\alpha}{3\pi}\left[\frac{p^2}{E_e^3}\right]\frac{1}{k} = \frac{2\alpha}{3\pi}\left[\frac{p^2\,2m}{E_e p^2}\right]\frac{1}{k} = \frac{4\alpha}{3\pi}\left[\frac{1}{E_e}\right]\frac{1}{k}$$

and if $W = E_e$ according to the assumption where $k \to 0$, one gets

$$\phi = \frac{4\alpha}{3\pi}\left[\frac{1}{W}\right]\frac{1}{k}$$

which is just the result of Iakobson's nonrelativistic calculation.

Expressions for the absolute and relative probabilities for the internal Compton effect have been derived for the magnetic 2ℓ multipoles by L. Spruch and G. Goertzel[13] using the Born approximation. On the basis of the internal conversion calculations, they have neglected the binding energy of the electron and restricted the process to account for only the K shell electrons. Additional assumptions treat the intermediate and final state of the electron as free and neglect terms in αZ as is consistant with the Born approximation. It is therefore expected that the calculations would be valid when the nuclear charge is small and the energy given up by the nucleus is at least the order of the electron rest energy. By dividing the probability for the internal Compton effect by the probability for internal conversion, it is unnecessary to evaluate the nuclear matrix elements, and, since the internal conversion probability was also calculated with the Born approximation, it is felt that this would be more valid since similar approximations are made in each calculation.

Their result for the 2^{ℓ} magnetic multipoles is

$$B(\ell,k,\theta) = \frac{\phi(\ell,k,\theta)}{\alpha_k(\ell,E)} = \frac{\alpha}{\pi^2 W^{\ell-1/2}\,(W+2)^{\ell+1/2}}\left(\frac{pq^2\,HF}{k}\right)dk \qquad (11)$$

where $H = (E')^{-2} [Wp^2 (1 - \cos^2\theta) + k^2 E'] - (E')^{-1} [kp^2 (1 - \cos^2\theta)$

$(k + p^2 + pk \cos\theta) q^{-2}] + k [kE' - p^2 k^2 (1 - \cos^2\theta) q^{-2}]$

$F = [(q^2 - W^2)^2 - (2W\alpha Z)^2]^{-1}$

$E' = E_e - p\cos\theta$

This differential internal Compton coefficient represents the ratio of the number of internal Compton electrons to the number of conversion electrons emitted by the same transition.

The L shell coefficient, according to Spruch and Goertzel, follows from the K shell coefficients by the replacement of Z by Z/2 if the 2p and small components of the 2s contributions are neglected. The spatial dependence of the 2s electron wave functions has been approximated by neglecting terms proportional in αZ. Therefore

$$\psi_{2s}(r,Z) = \psi_{1s}(r,Z/2)$$

and the L shell differential coefficients for the internal Compton effect become

$$B_L(\ell,k,\theta,Z) = B_K(\ell, k,\theta,Z = Z/2) \qquad (12)$$

We introduce the definitions for the differential magnetic internal Compton coefficient and the magnetic internal conversion coefficient

$$B_i = \frac{N_i(IC)}{N_i(CE)} \qquad \beta_i = \frac{N_i(CE)}{N} \qquad (13)$$

where $N_i(IC)$ and $N_i(CE)$ are the numbers of emitted internal Compton effect and internal conversion electrons respectively, and the subscript "i" is designated as either K or L depending on the atomic shell involved. N is defined as the number of gamma rays emitted from the same transition and in the same time.

The magnetic internal Compton coefficient for both the K and L shell contributions is then given by

$$B_{K+L} = \frac{N_K(IC) + N_L(IC)}{N_K(CE) + N_L(CE)} \tag{14}$$

and using equation (13) this becomes

$$B_{K+L} = \frac{N_K(IC) + N_L(IC)}{N\beta_K + N\beta_L} \tag{15}$$

Since the ratio of the magnetic internal conversion coefficient is

$$R = \beta_K/\beta_L \tag{16}$$

equation (15) becomes

$$B_{K+L} = \frac{N_K(IC)}{(R+1)\,N\beta_L} + \frac{N_L(IC)}{(R+1)\,N\beta_L}$$

Using equation (13) and equation (16), we get

$$B_{K+L} = \frac{R}{R+1}\,B_K + \frac{1}{R+1}\,B_L$$

or since

$$R = \frac{\beta_K}{\beta_L} = \frac{\frac{N_K(CE)}{N}}{\frac{N_L(CE)}{N}} = \frac{N_K(CE)}{N_L(CE)}$$

the differential probability for the internal Compton effect from both shells becomes

$$B_{K+L} = \frac{N_{K+L}(IC)}{N_K(CE) + N_L(CE)} \tag{17}$$

Where the probability of the internal Compton effect is defined as

$$\Psi_i = \frac{N_i\ (IC)}{N_T} = \frac{\text{probability for internal Compton effect}}{\text{probability that the nucleus makes the same transition}}$$

the differential probability involving both the K and L shells is

$$\Psi_{K+L} = \frac{N_K\ (IC) + N_L\ (IC)}{N_T} = \Psi_K + \Psi_L \qquad (18)$$

where Ψ_L is calculated by replacing Z by Z/2 in Ψ_K.

To apply Spruch and Goertzel's calculation to the electron energy spectrum of the internal Compton effect, it is necessary to integrate equation (11) over θ and multiply by the number of internal conversion electrons.

In the limiting case where $k \to 0$, the differential coefficient again reduces to the semi-classical result obtained by Chang and Falkoff for the bremsstrahlung associated with beta decay.

CHAPTER III

APPARATUS-SUPERCONDUCTING MAGNET SPECTROMETER

In recent years much effort has been expended to measure accurately electron spectra free from instrumental distortions. The developers of conventional magnet spectrometers have had considerable difficulty with scattering off focusing baffles and have had to resort to strong sources to provide adequate counting rates. The advent of silicon solid state detectors enabled measurements to be made at good resolution, but such spectra also include Compton distributions resulting from gamma rays scattered in the detector. In order to analyze electron spectra under conditions of minimum distortion, a superconducting magnet spectrometer has been developed. The use of this spectrometer, in conjunction with solid state detectors, combines the advantages of a true 4π beta ray spectrometer with the excellent energy resolution characteristic of silicon detectors. The complete collection of the emitted particles enables the use of very weak sources, and thereby reduces the scattering that might occur in the source itself. Summing the outputs of the detectors located at either end of the solenoid has eliminated all distortion from electron backscattering. This allows the quantitative analysis of small effects that otherwise might be hidden in an instrument-produced background. Since the flux of gamma rays is not inhanced by the application of a

magnetic field, the Compton distribution resulting from interactions in the detectors has been almost totally eliminated.

Description of Equipment

The general detail of the apparatus, as illustrated in figure 2, consists of three dewars, the magnet, and a probe containing the detectors and source. The two outer dewars are used for the nitrogen and helium supply, respectively, and are of conventional design with the constraint that their diameters permit insertion of the magnet. The inner dewar is constructed of thin-wall stainless steel and is evacuated with an ion pump to 5×10^{-7} torr. The inner dewar is designed to pass through the center of the solenoid and extend beyond the level of the liquid helium. Its function is to provide insulation of the detector probe from the helium bath. The solenoid, containing the probe, is illustrated in figure 3. The source, mounted on 1/4 mil aluminized milar film, is positioned along the axis and at the midpoint of the magnet.

With the field directed parallel to the axis, the electrons emitted from the source are constrained to follow helical orbits to either of the detectors. If a particle backscatters off one of the detectors, it spirals down the field in the opposite direction to be coincidently absorbed by the other detector. Since the detector outputs are summed, this arrangement adds the pulses arising from the initial and backscattering events to yield a pulse representive of the total energy absorbed by the detectors. In contrast, the efficiency for gamma rays is limited to the solid angle subtended by the detectors.

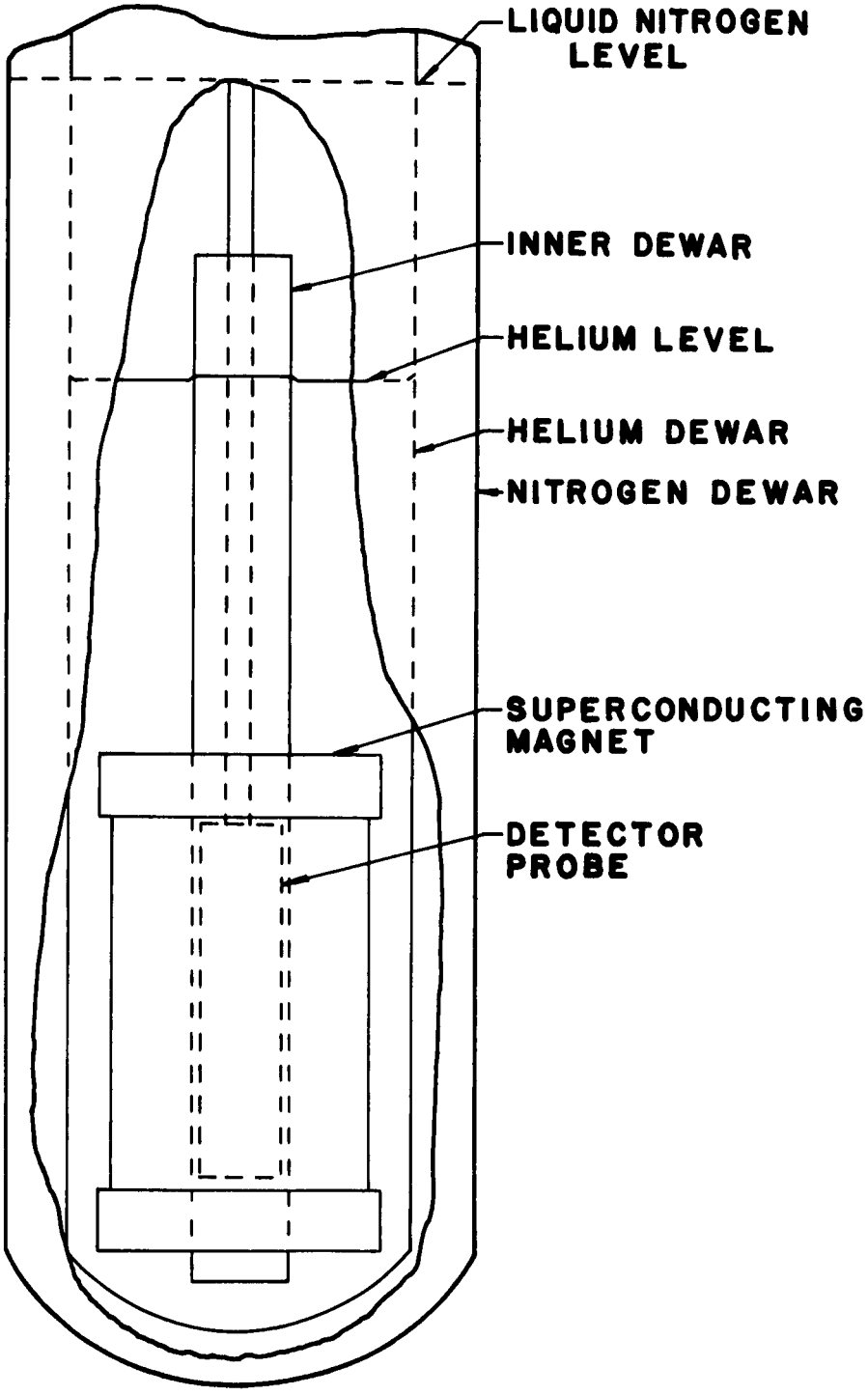

Fig. 2. Superconducting magnet spectrometer

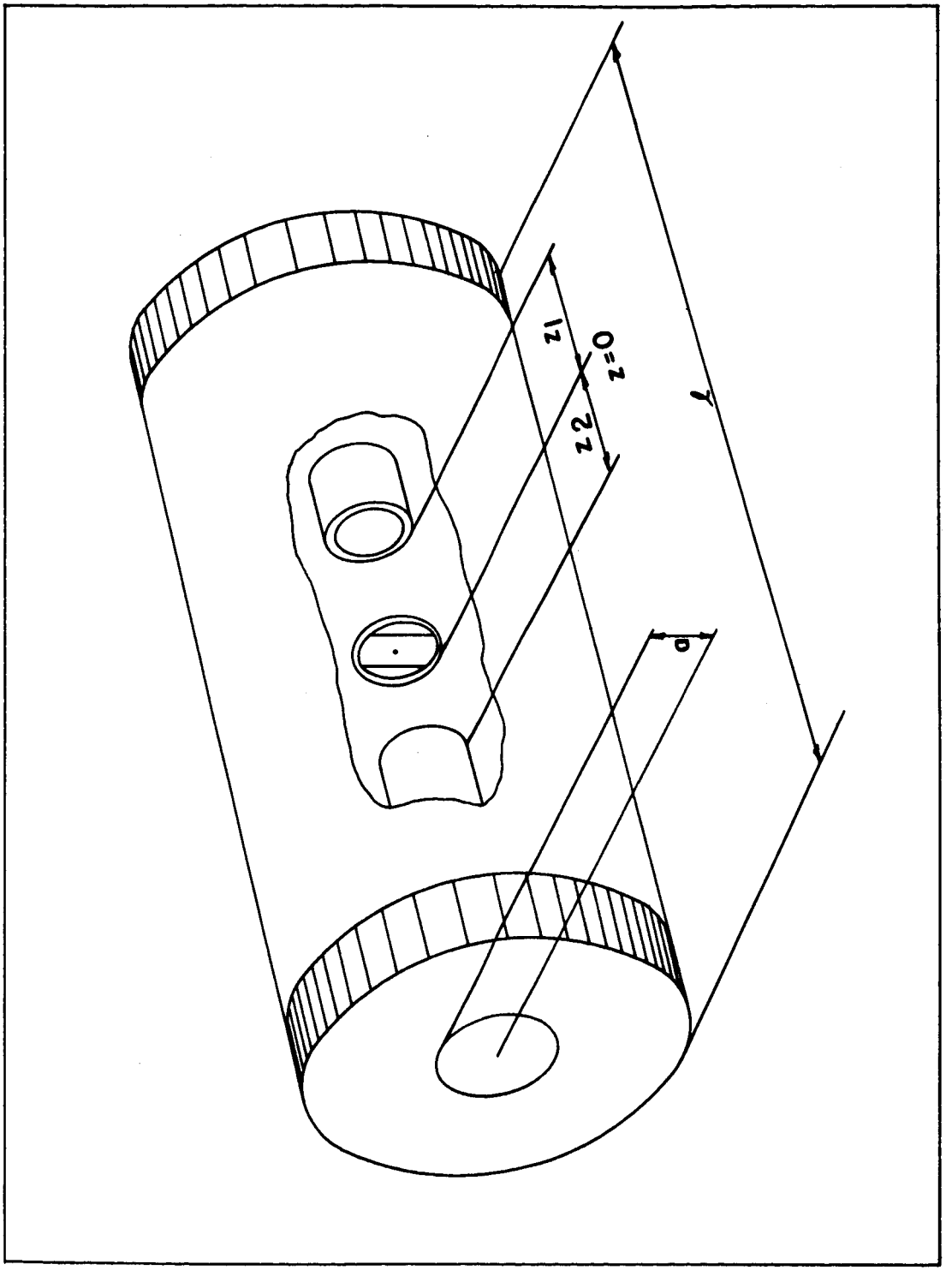

Fig. 3. Arrangement of detector probe in solenoid.

With the geometry used in the experiments, the ratio of complete collection to the two solid angles yielded an efficiency of charged particles over gamma rays of approximately 3×10^4 per cent.

The superconducting solenoid must meet three requirements:

1. The radius a of the working volume must be much less than the length ℓ to ensure a uniform field and still provide room for the probe and insulating dewar.
2. The length ℓ must be sufficiently long to allow a favorable solid angle ratio for the supression of the gamma ray distribution without including the area where the distorting end effects become significant.
3. The magnet must be capable of producing fields strong enough to confine the electrons to a radius not larger than that of the detectors.

For the solenoid spectrometer used, condition (1) was easily met. Referring to figure 3, a = 2.54 cm, ℓ = 20.3 cm, and the ratio ℓ/a = 8.0. Condition (2), however, is not so clearly satisfied; a calculation of the axial magnetic field was made to insure that at least the minimum field for focusing the electrons be present in the region of the detectors. Referring again to figure 3, the positions of the solid state detectors relative to the center of the solenoid are z_1 = 8.9 cm and z_2 = -6.9 cm. The axial magnetic field of a solenoid, as a function of the distance (measured from the center) along the symetry axis, is given by[14]

$$H_Z = \frac{I}{2\ell}\left[\frac{(Z_i + \ell/2)}{[a^2 + (Z_i + \ell/2)^2]^{1/2}} - \frac{(Z_i - \ell/2)}{[a^2 + (Z_i - \ell/2)^2]^{1/2}}\right] \quad (19)$$

This relation has been numerically evaluated, and with the field normalized to unity at the center of the solenoid, the results graphed in figure 4 were obtained. The range of the detector positions is shown by the corss-hatched area. In these positions, the field at the detectors is maintained at a value greater than 75% of the maximum available field.

The electrons, emitted by the source at the center of the solenoid, follow a helical path in the magnetic field. The axis of the helix is displaced from the axis of the solenoid by the radius of the helix. This radius may vary from zero, which corresponds to the electron being emitted directly down the axis of the solenoid, to some radius r_m, which corresponds to the electron being emitted normal to the axis.

In the latter case, two effects must be considered.

(1) The electrons may have such a large radius of curvature that they may not be incident upon the detector.

(2) The component of velocity along the axis of the solenoid may not be large enough to collect all of the charge within the integration time of the amplifier. This is of particular concern where the two detectors at either end are run in parallel, with their outputs summed as the electron scatters from the detector at one end to the detector at the other. It must then traverse the length of the solenoid in a time which is short compared to the integration time of the amplifier.

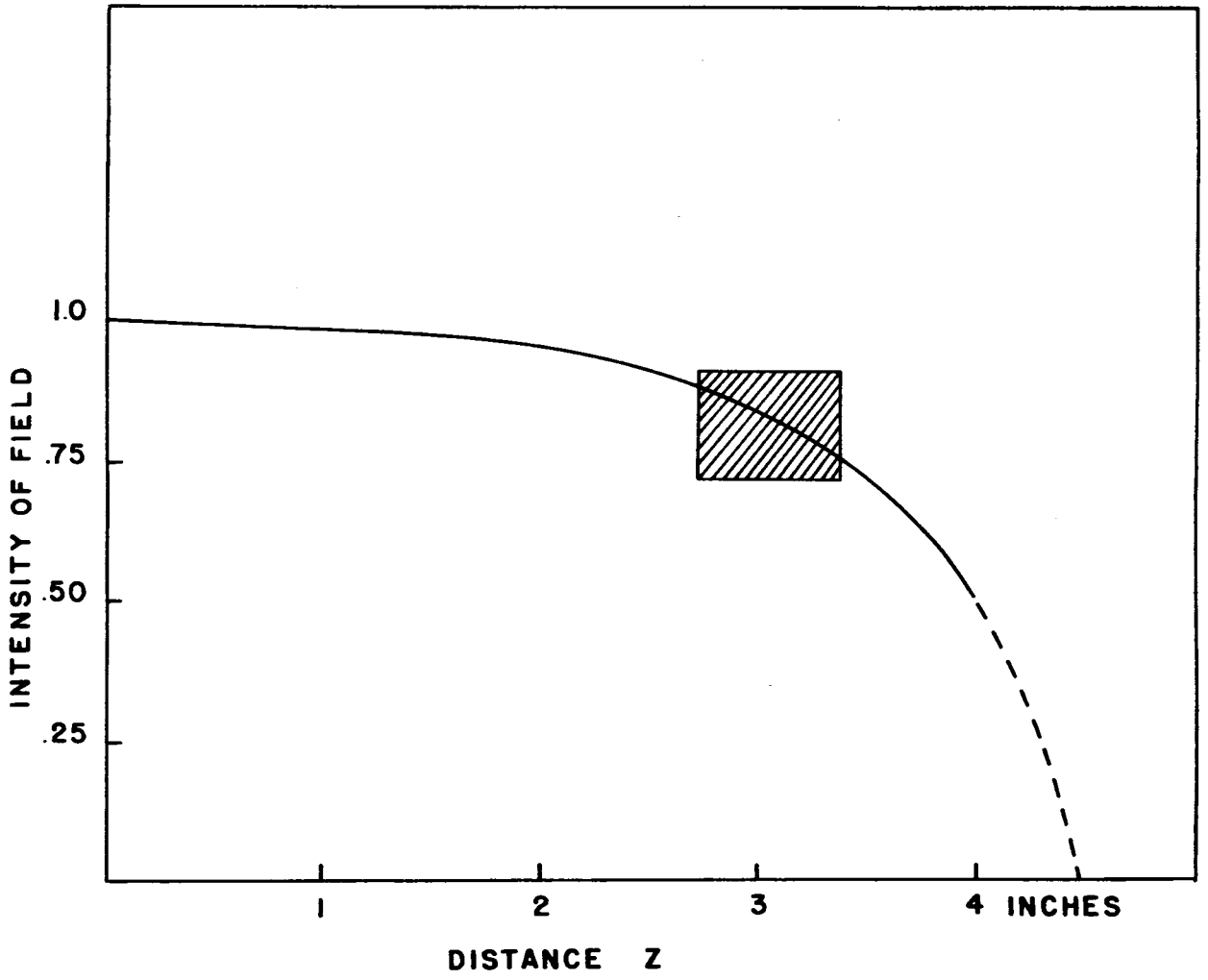

Fig. 4. Magnetic field intensity along axis of solenoid. The cross hatched region corresponds to the position of the detectors.

The first effect depends upon the size of the magnetic field and the dimensions of the detectors. A charged particle with a momentum p in the direction normal to a magnetic field B, is constrained to move in a circle of radius r, as defined by $p = (Be)\, r$ where e is the electronic charge. This radius will vary from zero to some maximum radius r_m depending on the component of momentum perpendicular to the field. In the superconducting magnet spectrometer, the electron will have the maximum radius when it is emitted from the source in a direction normal to the magnetic field of the solenoid. Since $E = T + 1$, $E^2 = (T + 1)^2$ and using the relationship $E^2 = p^2 + 1$ the maximum radius that a particle of kinetic energy T, emitted normal to the field B, can attain is

$$r_m = p/Be = \frac{(T^2 + 2T)^{1/2}}{Be} \tag{20}$$

The maximum radius r_m as a function of the electron energy and the magnetic field has been calculated and is shown in figure 5. For the detectors used, the spectrometer was operated in the cross-hatched region. The superconducting magnetic was capable of 30 kilogauss, and the experiments run at 25 kilogauss.

The second effect is more serious since the full energy of some electrons will never be detected. In calculating the importance of this effect, the assumption is made that the particles are initially emitted from the source in an isotropic distribution. Then the total number of particles emitted is proportional to the surface area of a sphere, concentric with the source. This sphere is shown in figure 6 with the additional assumption that the source is a point source.

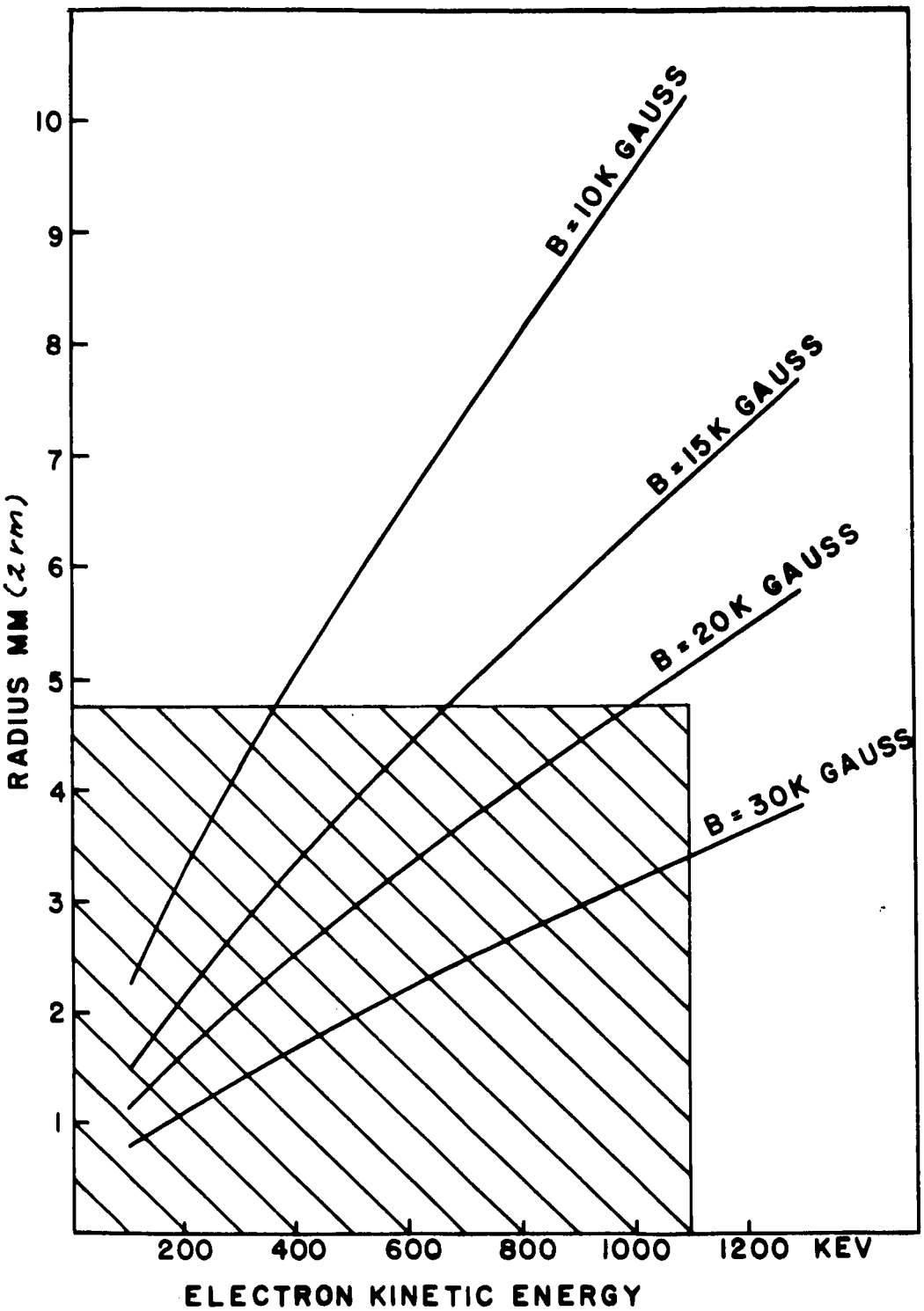

Fig. 5. Maximum electron radius for a particle emitted perpendicular to the magnetic field $\vec{B}$.

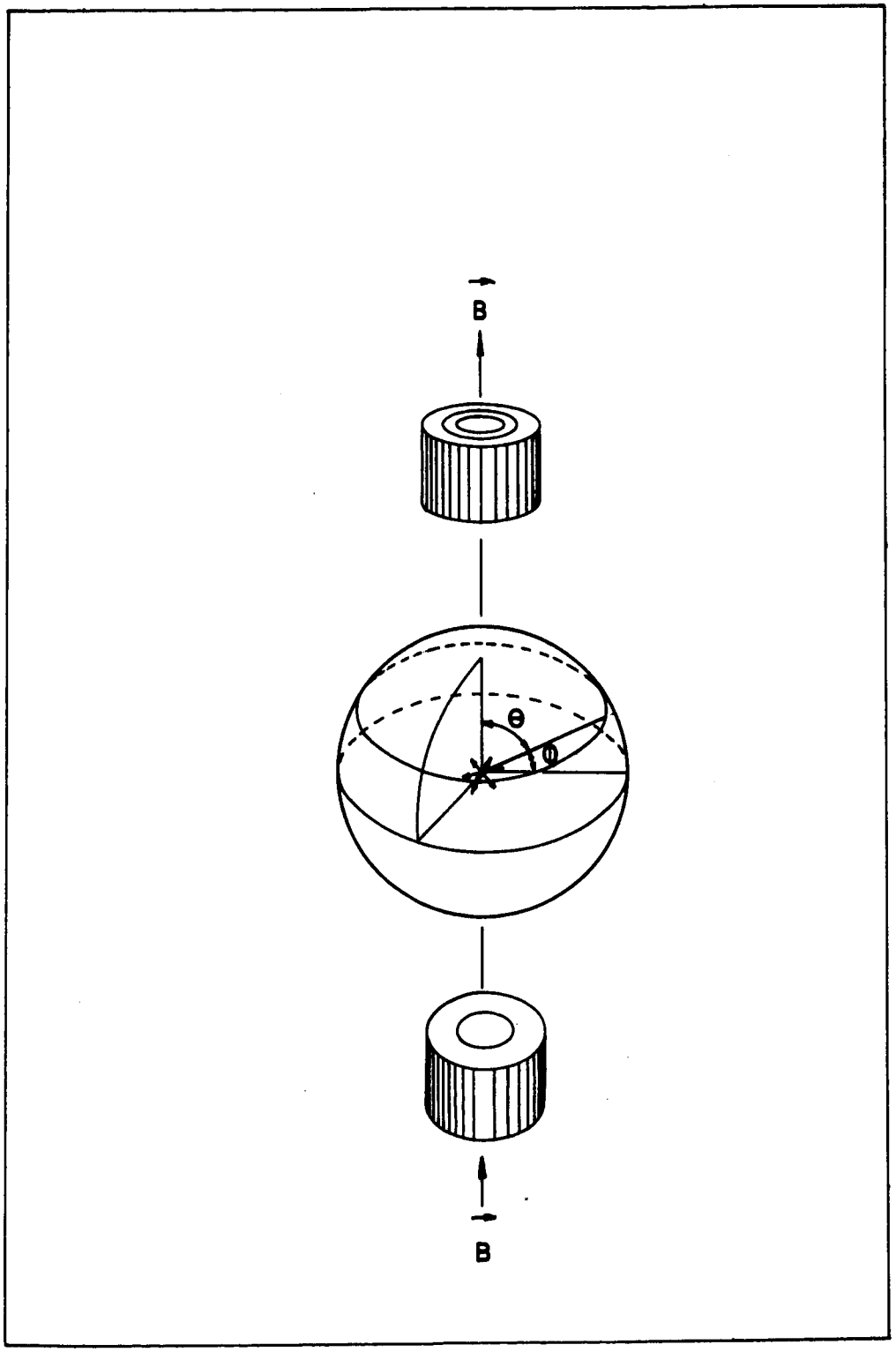

Fig. 6. Assumptions for calculating the fraction of the electrons emitted within an angle ϕ .

This last assumption is a good one since the total source intensity needed is only a few nanocuries. This means that the source area can be much smaller than that used in other types of spectrometers and, in our case, it is usually less than 1 mm^2. Therefore, the number of particles emitted within an angle $\phi = 0$ to $\phi = \pi - \theta$ where θ is measured with respect to the axis of the solenoid, is proportional to the fraction of the sphere swept out by rotating around the axis. Performing the integration, the number emitted with this angle is proportional to $\cos \theta$.

The time of flight of the particles is determined by their component of velocity, v_z, parallel to the field, and by the distance from the source to the detector. This time of flight, t, is given by

$$t = z/v_z$$

The kinetic energy of the particles is

$$T = \frac{mc^2}{\sqrt{1 - \beta^2}} - mc^2$$

where $\beta = v/c$

Therefore, solving for β_z, equation becomes

$$\beta_z = v_z/c = \left[1 - \frac{1}{\left(\frac{T_z}{mc^2} + 1\right)^2}\right]^{1/2}$$

and since

$$T_z = T \cos^2 \theta$$

$$N = \cos\theta = \left[\frac{mc^2}{T}\left(\left(1-\left(\frac{z}{ct}\right)^2\right)^{1/2}-1\right)\right]^{1/2} \qquad (21)$$

where t is the collection time of the detecting system, in this case, the integration time of the amplifier. In figure 7, this fraction, expressed as a percentage, has been ploted as a function of integration time for different electron energies. Only one traversal from the source to the detector has been considered. However, for integration times the order of one microsecond, this fraction is still quite small for several traversals.

Figure 8 is a block diagram of the electronics. The use of a multichannel analyzer eliminates the necessity of taking a spectrum point-by-point as is required in other spectrometers. The collection efficiency is such that even with a 20 nanocurie source, run times were usually 40 minutes or less.

Operation and Experiments

The initial experiments were performed using one detector at a time to observe the conversion electron spectrum of Bi^{207}. Since Bi^{207} decays from the ground state to the excited states of Pb^{207} by electron capture, there is no competition with the conversion or internal Compton spectrum from a beta branch. Of the five gamma rays, the 570 keV, pure electric quadrupole is the most intense, followed by the more highly converted 1064 keV, magnetic octupole transition. The high internal conversion coefficients for this well known nucleus make it ideally suited for investigating the operation of the superconducting magnet spectrometer. The increase in collection with the field

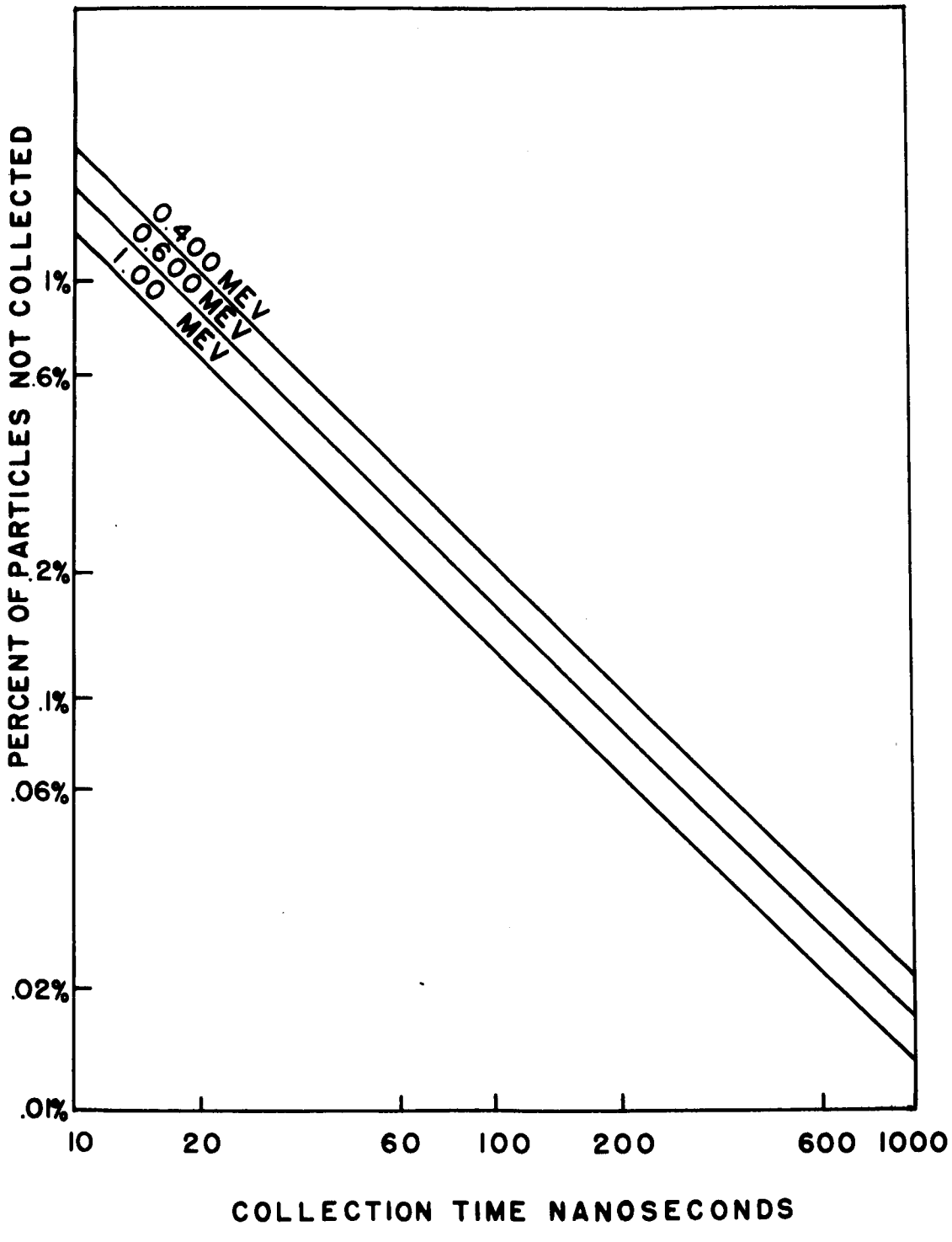

Fig. 7. The percentage of the emitted particles not collected within the integration time of the amplifier.

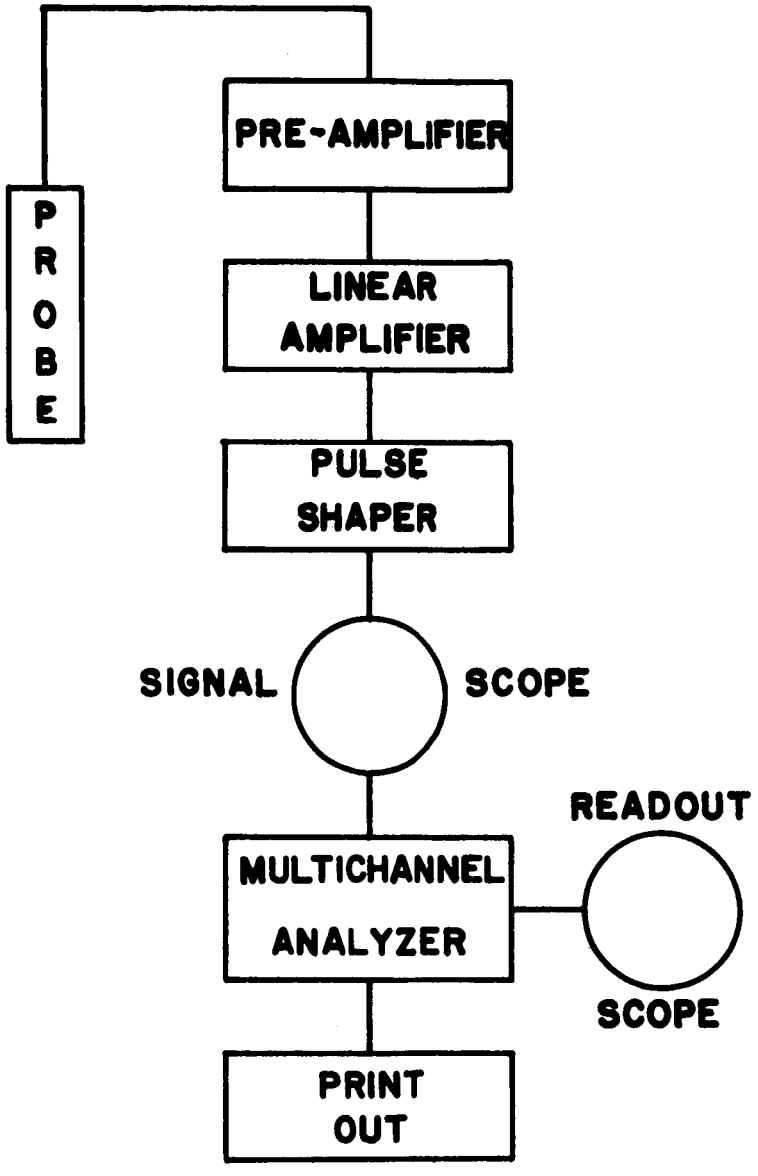

Fig. 8. Block diagram of the electronics used with the superconducting magnet spectrometer.

on is in agreement with the source strength, as determined by knowing the specific activity and the amount of material pipetted onto the source-backing.

Compared in figure 9 are the spectrums with and without the field, as seen with one detector. It shows that the Compton distribution has been significantly reduced, but that the backscattering tail is still evident.

With two detectors in parallel, this tail should be eliminated since the scattered electron is in coincidence with the energy retained in the first detector. In figure 10 the spectrum taken with this arrangement is shown. It is evident that there remains a low energy tail on the distribution. We have investigated this portion of the spectrum and find it to be consistent with several calculations of the internal Compton effect. We believe this to be the first direct spectral observation of this phenomenon.

In any experiment where the effect under consideration is small, it is necessary to determine whether the contribution from background is significant. The region from channel 100 to 160 (in figure 10) has been expanded, and is plotted in figure 11. Two additional sets of data are shown. A spectrum was measured with the superconducting magnet turned off, and a background spectrum of nearly constant amplitude, approximately 1% of the field-on spectrum, was observed. To determine the contribution of any gamma ray events, aluminum absorbers were placed before the detectors to absorb any beta rays. Both background spectrums have been measured well below the peak of the internal conversion line where the spectral distribution would be expected to

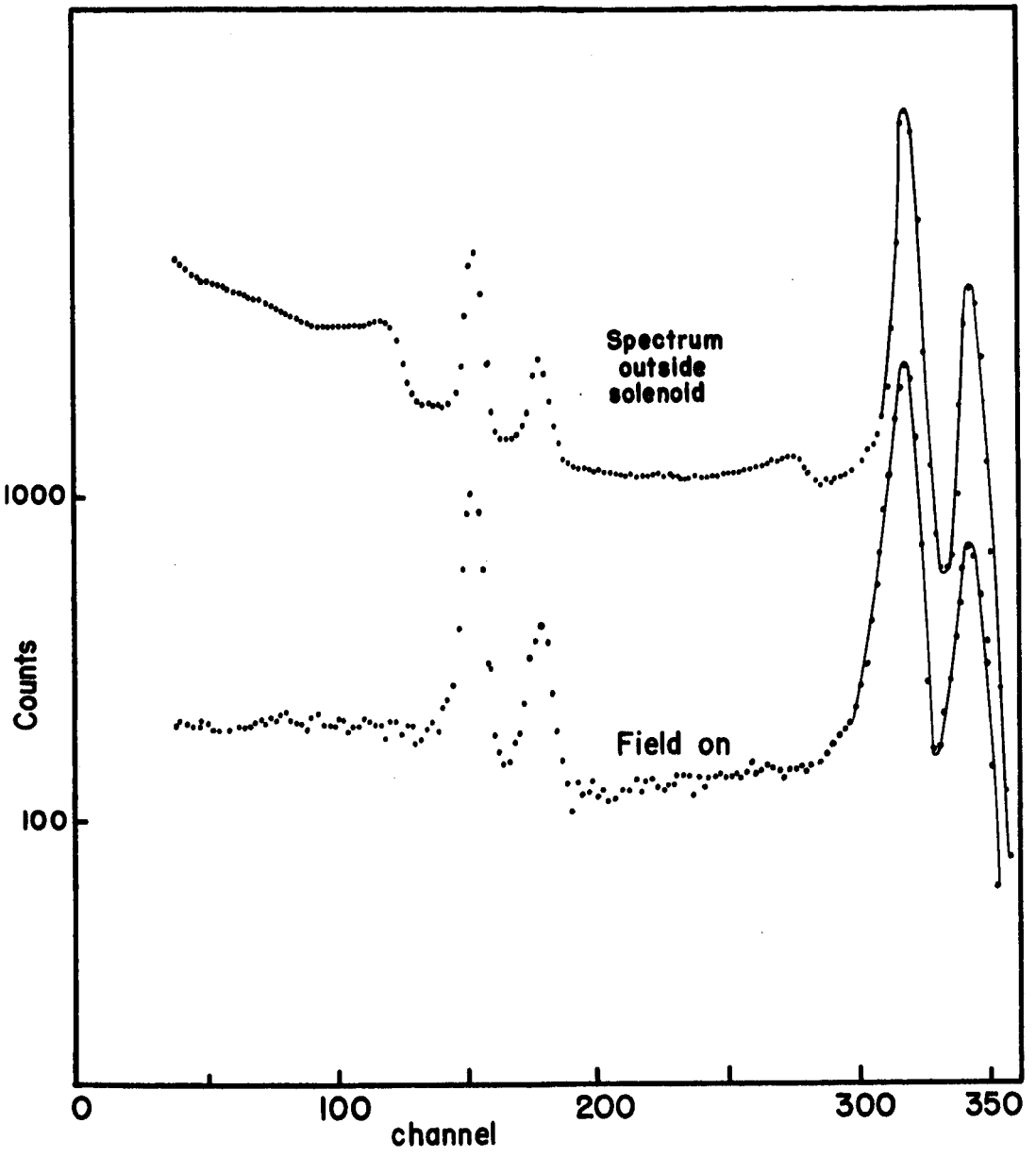

Fig. 9. Data taken with one detector, with and without the field.

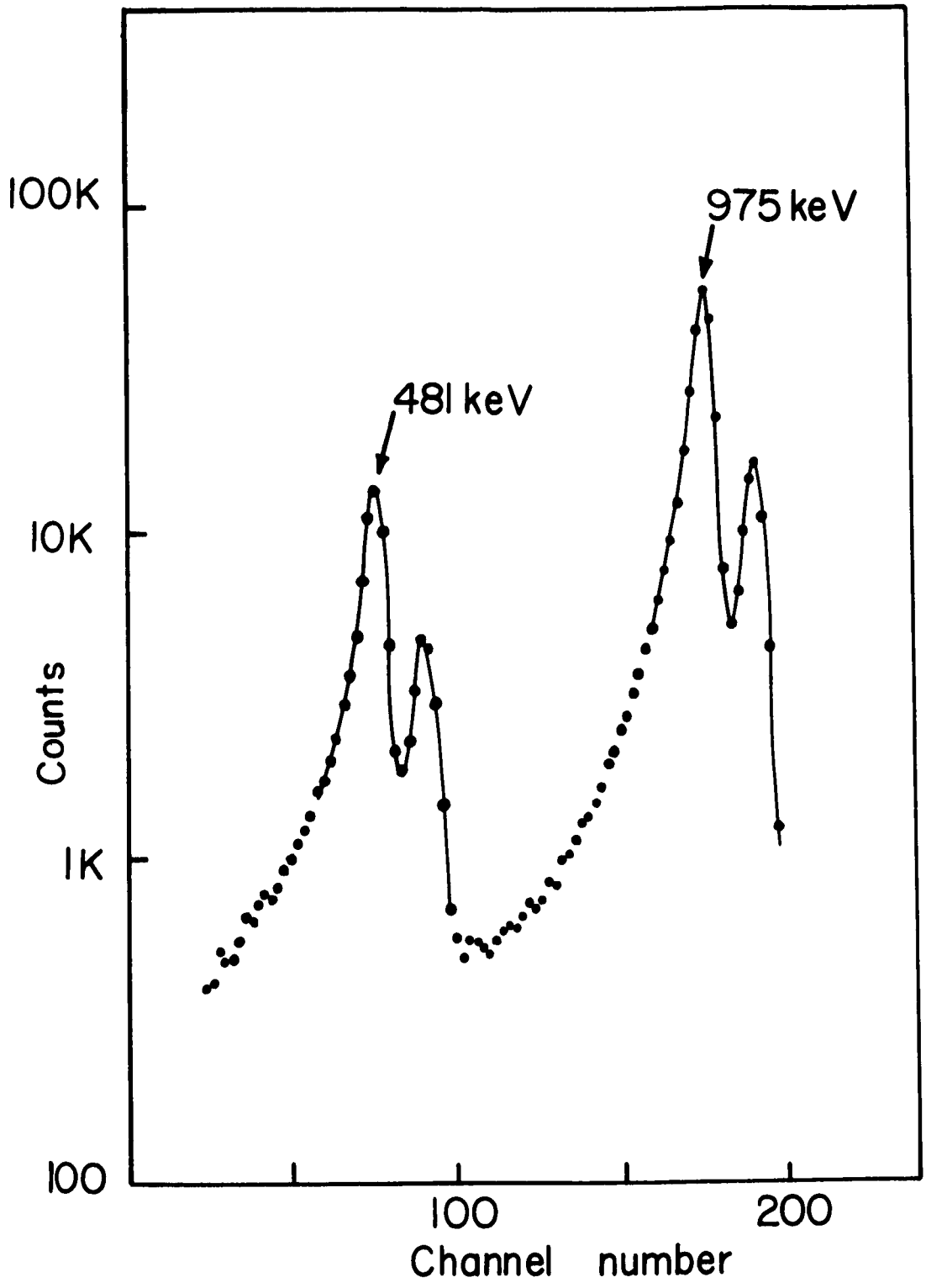

Fig. 10. Data taken with the magnetic field and two detectors in parallel.

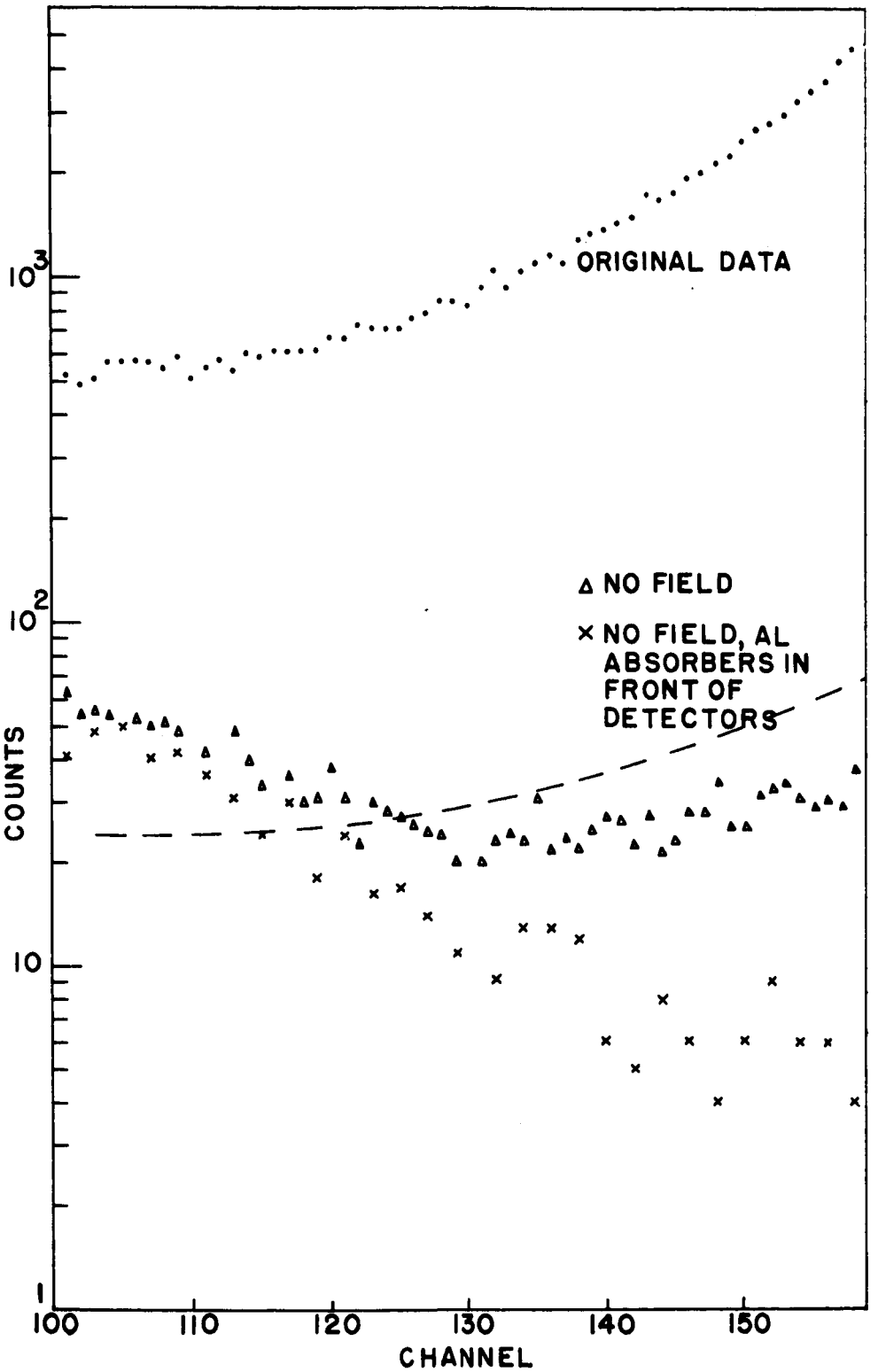

Fig. 11. Comparison of the background spectra to the data. The dashed line represents the standard deviation of the data.

result from the internal Compton effect. The dashed line represents the standard deviation of the counds in the field-on spectrum and indicates, by comparison, the negligible contributions of the background and gamma ray spectrum.

Conclusion

The superconducting magnet spectrometer, when operated in conjunction with silicon solid state detectors, provides a new method for analyzing electron spectra under conditions of minimum distortion from gamma or backscattering distributions. The instrument has the advantage of being relatively compact and requiring little supporting equipment. Its operational capabilities have been investigated primarily in the observation of the internal conversion spectrum and the internal Compton effect, but its applicability exists wherever it is desired to study electron spectra at the high resolution afforded by solid state detectors.

CHAPTER IV

ANALYSIS

In order to apply any of the theoretical calculations for the internal Compton effect to the observed data it is necessary to ascertain the intensity of the internal conversion line for each transition, and to account for the amount of distortion the finite linewidth of the detectors introduces into the spectrum.

Since the superconducting magnet spectrometer provides complete collection of the emitted particles, the intensity of the conversion line has no dependence upon the efficiency or solid angle of the detectors. In the case of a continuous spectrum, however, it is necessary to make a judgment on the extent of the conversion line. This was established by folding the high energy side of the conversion peak symmetrically onto the low energy side, with the assumption that the high energy side is free from any distortion aside from the resolution of the detectors. The peak so generated in this process is illustrated in figure 12 for the 975 keV conversion line.

The reliability of this method was checked in two ways. The conversion line intensities, represented by the area under each peak, and the accepted values for the conversion coefficients can be used to calculate the total intensity of the transition. This was performed

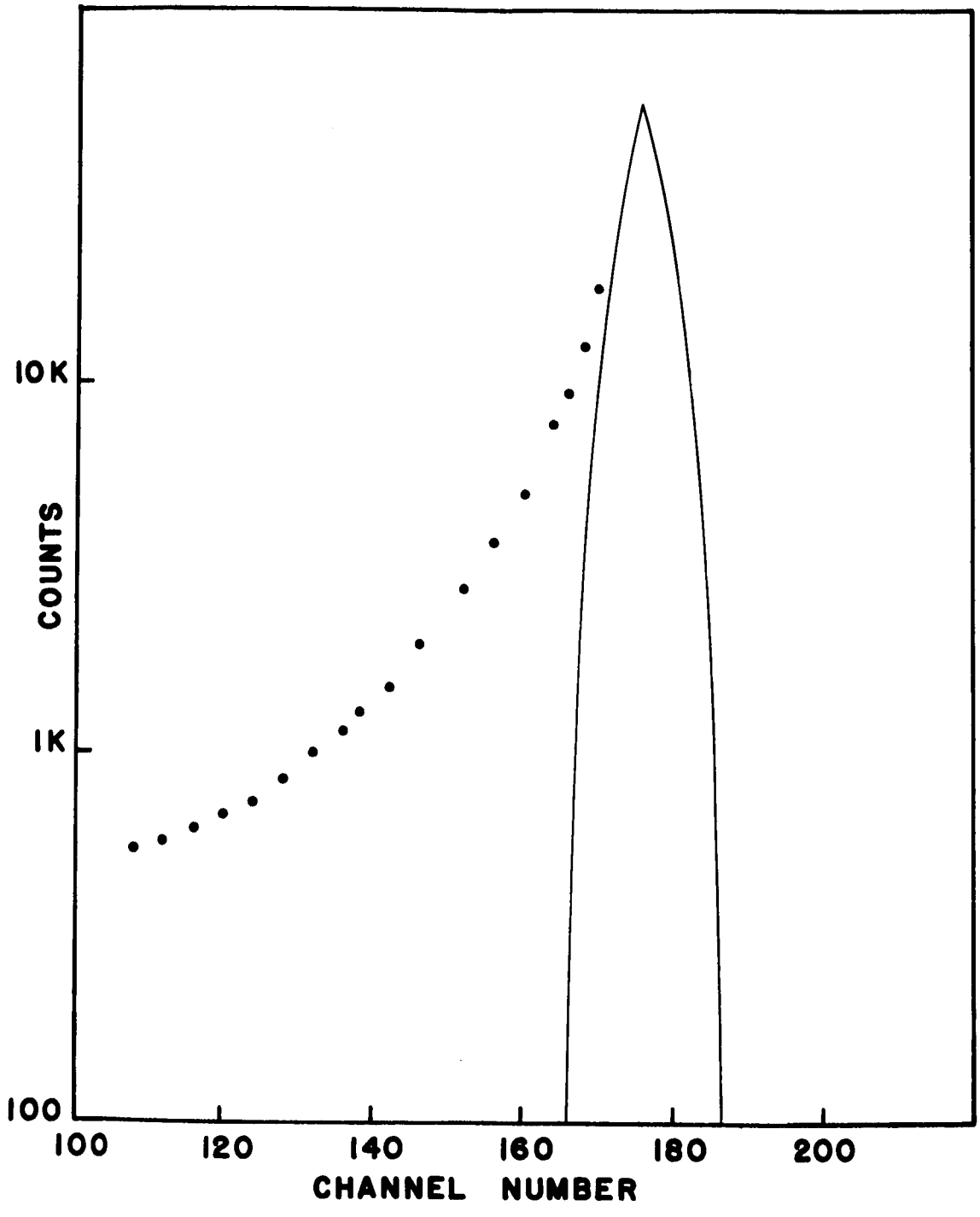

Fig. 12. Internal conversion line shape determined by folding over the high energy side of the peak.

for both the 975 and 481 Kev conversion lines and the ratio of these intensities compares favorably with the reported values. The K/L ratio, defined as the number of conversion electrons ejected from the K shell, divided by the number ejected from the L shell, can be compared with other experimental and theoretical values for each transition. A comparison of these checks is made in Table I and II.

It is possible for the linewidth of the detectors to distort the spectrum because the number of counts registered in any energy interval, or channel as it is represented on a multichannel analyzer, is only proportional to the number of particles which actually had that energy on entering the detector. Consider figure 13. If one assumes a monoenergetic source, such as an idealized conversion line of intensity $\eta_T(I)$, where I represents an index on the energy interval, then the effect of a detector with a finite resolution is to spread these counts over a number of channels each with an intensity $\eta_o(I)$. Assuming that no particles escaped the detector, the sum of the broadened distribution should equal the intensity of the monoenergetic line. This can be expressed as

$$\eta_T(I) = \sum_{k=-n}^{n} \eta_o(I + K) \qquad (22)$$

where 2n equals the number of channels over which the detector distributed $\eta_T(I)$.

When this analysis is applied to a continuous distribution of incoming particles, the net effect is that the detector only records a fraction of the counts that entered within the energy interval I, but

TABLE I

TRANSITION	$\frac{N_K(CE)}{N_{LM}(CE)}$	THEORETICAL K/L RATIO	OTHER EXPERIMENTAL K/LM RATIOS
1064 keV 975 keV(CE)	3.19	3.74[15]	3.35[16] 3.40[17]
570 keV 481 keV(CE)	2.45	3.1[15]	2.07[16] 3.0[17]

TABLE II

TRANSITION	$\frac{N_T(1064\ keV)}{N_T(570\ keV)}$	OTHER EXPERIMENTAL INTENSITY RATIOS	THEORETICAL INTENSITY RATIO
$\frac{1064\ keV}{570\ keV}$	0.80	0.87[17]	0.925[15]

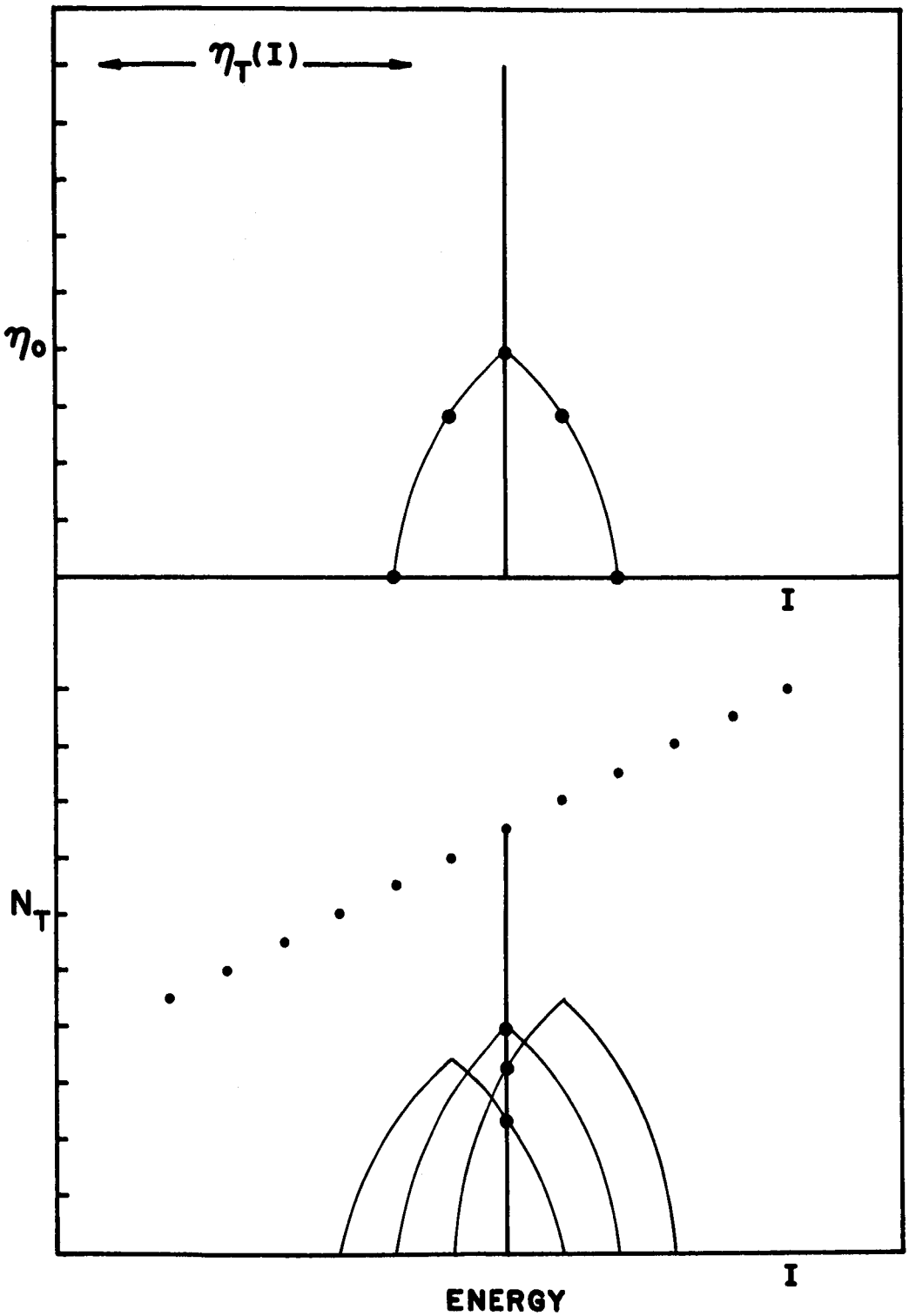

Fig. 13. The effect of detector resolution on an idealized conversion line and a continuous distribution.

adds to this contributions from adjacent channels. Thus the number of counts, $N_o(I)$, displayed on the analyzer is given by

$$N_o(I) = \sum_{k=-n}^{n} F(k)N_T(I+k) \qquad \text{with } F(k) = \frac{\eta_T}{\eta_o} \frac{(I)}{(I+k)} \tag{23}$$

where 2n is the resolution of the detector in channels as determined by observing the distribution of a monoenergetic conversion line. Provided the resolution of the detector is relatively constant over the energy range under consideration, the theoretical distributions, $N_T(I)$, can be corrected for this effect by applying equation (23) to fold in the resolution of the detectors. If the slope of the theoretical distribution does not vary too greatly over the number of channels corresponding to the energy resolution, folding in the resolution will have little effect. This calculation was performed for 19 theoretical spectra with less than a 2% change in the region of interest.

In an analytical comparison of the theoretical work with the experimental data, three characteristics should be evaluated: the intensity of the effect should agree in magnitude with the data to demonstrate that the distribution observed is actually the internal Compton effect; the energy distribution should be considered to reveal any discrepancies or similarities in shape with the data or other calculations; the multipolarity dependence should be investigated to determine whether a unique assignment can be given to a transition on the basis of the theoretical calculation.

The theoretical calculations for the internal Compton effect involving K shell electrons are compared to the observed data in figure 14.

In evaluating these results, it is necessary to restrict the comparisons to the energy range below the internal conversion line. As in figure 12 for the 975 keV conversion line, this range may extend up to channel 166, but on the basis of the line folding considerations, the validity of the results are restricted to below channel 160 for the M4 transition and below channel 60 for the E2 transition.

For the calculation of Spruch and Goertzel, the Born approximation requires that the electron momentum, p, obey the relationship $p \gg \alpha Z \sim 0.6\ mc^2$. This is violated for Bi^{207} in the region of interest, but the agreement at higher energies may be explained by this inequality improving as the energy approaches that of the conversion line. Spruch and Goertzel expect close agreement with experimental data because they have calculated a relative probability coefficient, i.e., the probability of the internal Compton effect divided by the probability for internal conversion. Since both calculations are performed in the Born approximation, errors resulting from the approximations may have been lessened and agreement is expected at least in the range where the Born approximation is able to predict accurate values for the internal conversion coefficients.

The theory of Baumann and Robl yields relatively good agreement with the data for the magnetic transition but much less satisfactory results for the electric transition. Their work was performed under

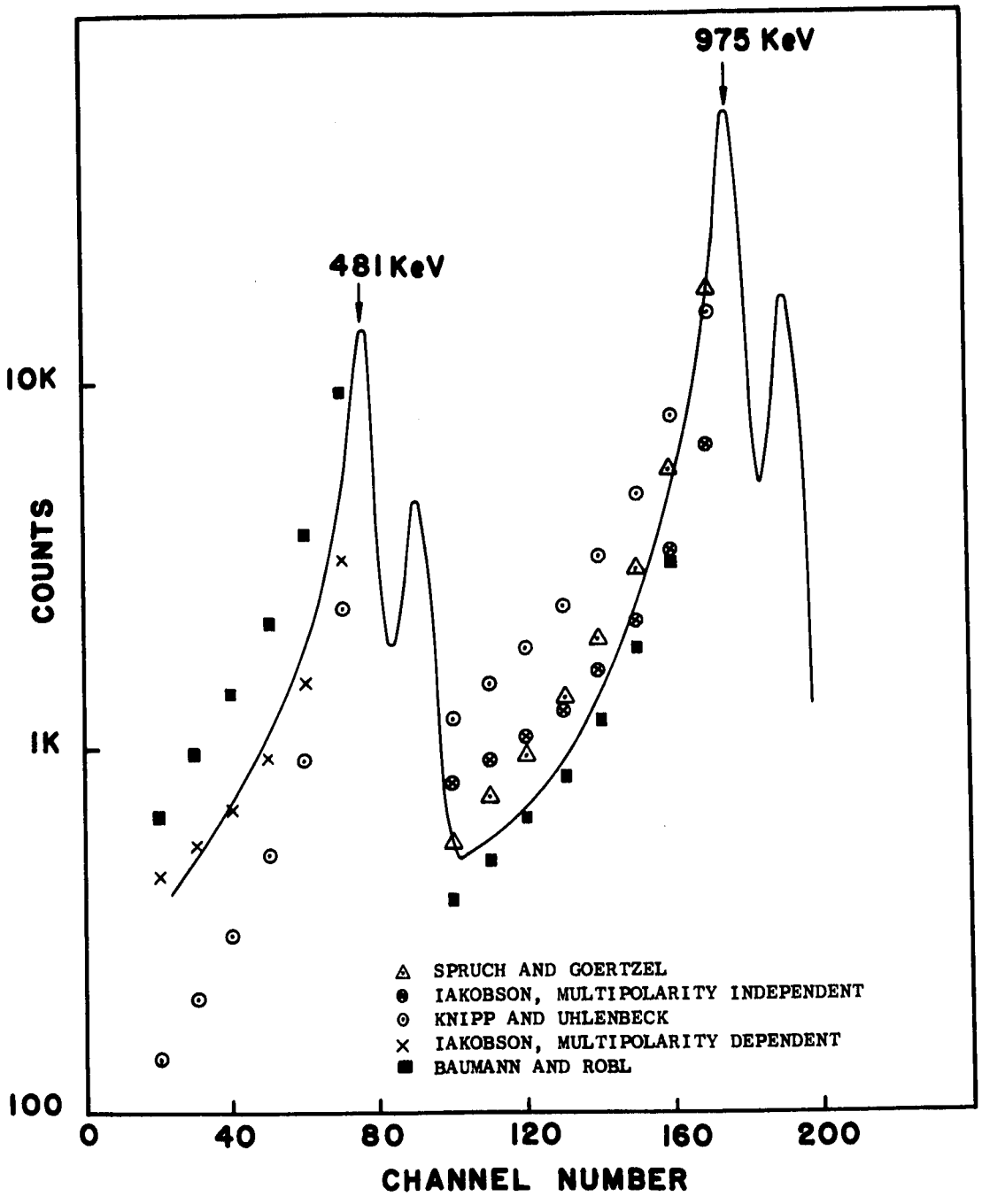

Fig. 14. Comparison of the K shell theoretical calculations for the internal Compton effect with the data.

the requirement that $k \gg \alpha Z \backsim .6\ mc^2$ which is not satisfied for either transition. To calculate the intensity of the internal Compton effect from their work, it is necessary to multiply the probability coefficient, ψ, by the number of decays, both electron and gamma, undergone by the transition under study. This number can easily be obtained if one knows the internal conversion coefficient, α_K, and the number of conversion electrons emitted. Since $\alpha_K = N_K(CE)/N_\gamma$ therefore $N_\gamma = \frac{N_K(CE)}{\alpha_K}$ and the total number of transitions $N_T = N_K(CE) + N_\gamma$ is given by

$$N_T = N_K(CE)\ (1 + 1/\alpha_K) \tag{24}$$

It should be noted that any error in the experimental values for $N_K(CE)$ or α_K will signigicantly alter the intensity of the result. However, the more serious problem is probably the violation of the requirement $k > \alpha Z$ by application of this theory to Bi^{207}.

Iakobson has calculated the internal Compton effect nonrelativistically with the requirement that $W \ll mc^2$. This inequality is not satisfied for either transition considered. It was not possible to apply the multipolarity dependent calculation to the M4 transition because the gross violation of the energy requirement yielded a meaningless answer. It was possible, however, to apply the Z and multipolarity independent formula with relatively good agreement. In this formula Iakobson, like Spruch and Goertzel, divides the probability for the internal Compton effect by the nonrelativistic probability for internal conversion. The agreement of Iakobson's calculation, even with such large violations in the energy and Z requirements,

indicates that this type of calculation may have a greater range of validity and may be less sensitive to the approximations than the expressions relating the internal Compton effect to the probability of a nuclear transition. For the electric transition, the multipolarity dependent and the multipolarity independent formula of Iakobson yield identical results that are in good agreement with the data.

The bremsstrahlung calculation by Knipp-Uhlenbeck shows the largest variation in intensity from the data. This is probably due in part to the assumption that Z = 0 and to the fact that the calculation is independent of the multipolarity of the transition.

In order to accurately compare the data with the theoretical predictions, it is necessary to take into account the contribution from the L shell electrons. Spruch points out the L shell coefficient may be calculated by replacing Z by Z/2 and including the change in binding energy in equation (11). Figure 15 illustrates the result of these calculations. The dashed line represents an assumed shape for the L distribution as determined by normalizing the K and L shell conversion peaks and assuming the same energy dependence. For both transitions, neither theory seems to be in agreement with each other or what might be expected for the L shell contribution. On the basis of these curves, it seems that equation (12) cannot adequately predict the magnitude or the energy dependence of the L shell internal Compton effect.

Figure 16 indicates the effect of considering the contribution of the L shell to the theoretical predictions. This has increased the agreement of Baumann and Robl's calculation for the magnetic transition, but lessened that of Spruch and Goertzel's. The calculations of Knipp

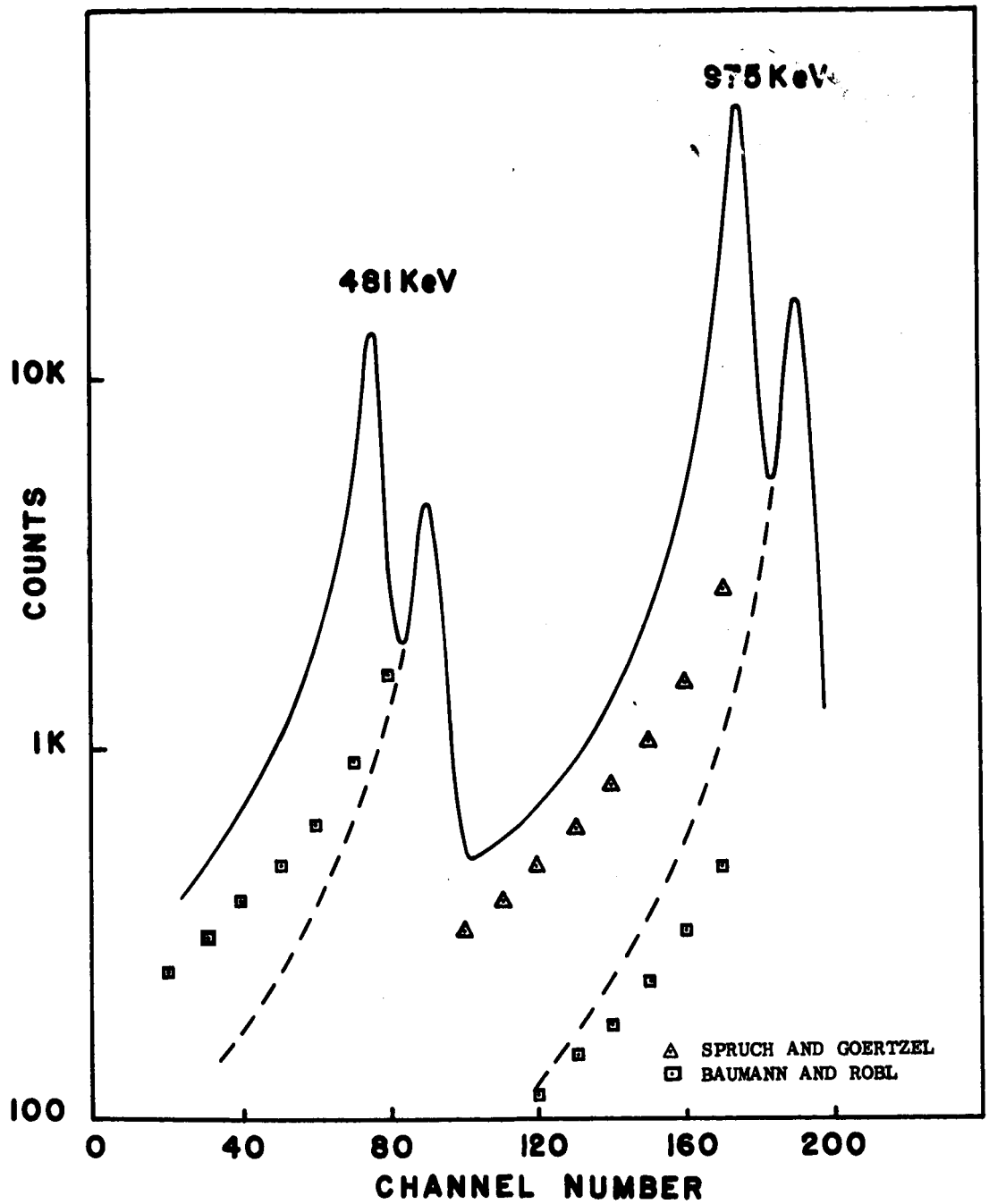

Fig. 15. Comparison of the L shell theoretical calculations for the internal Compton effect with the data.

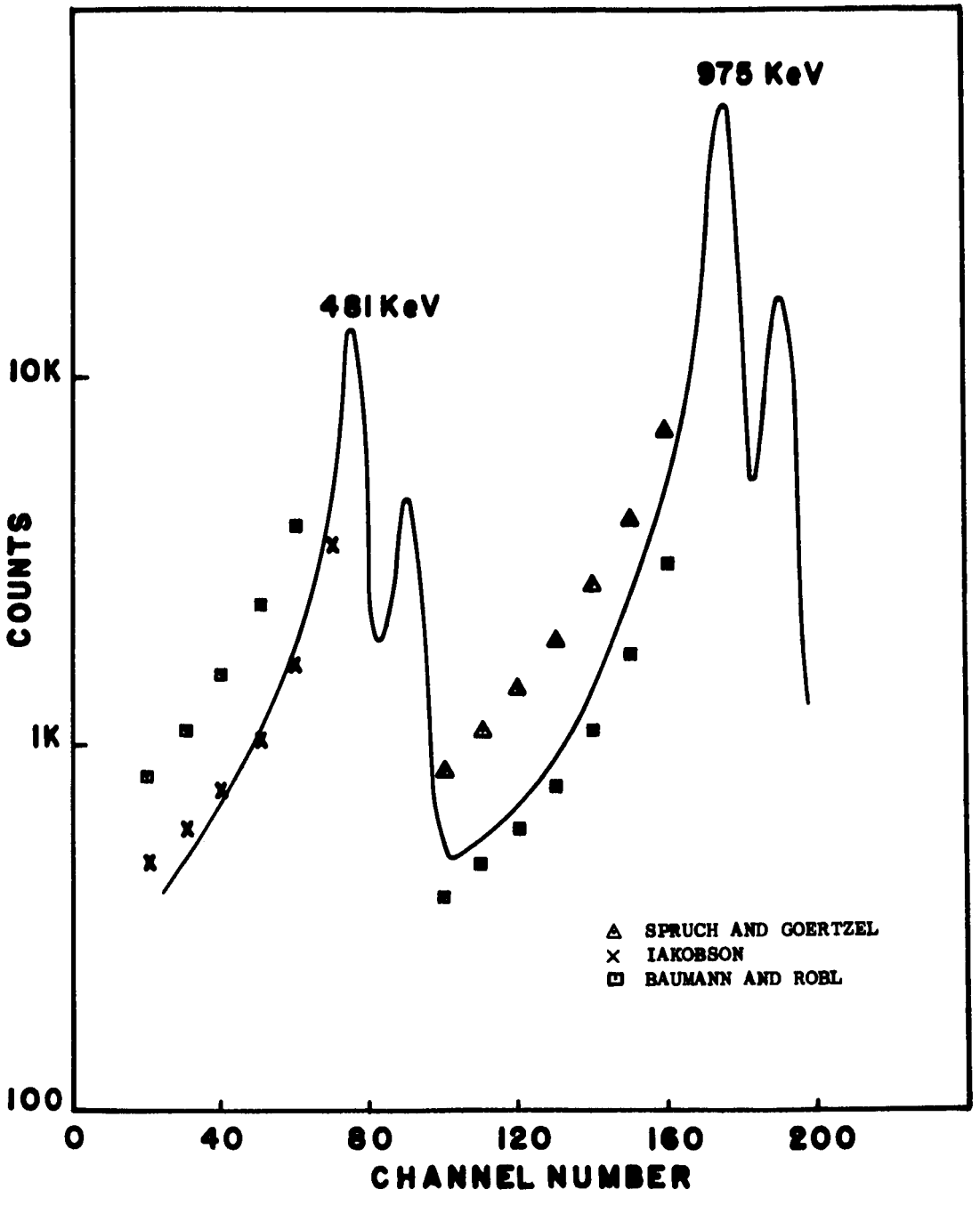

Fig. 16. Comparison of the K+ L shell theoretical calculations for the internal Compton effect with the data.

and Uhlenbeck and the multipolarity independent formula of Iakobson have not been included because they have no dependence upon Z and the L shell contribution could not be calculated.

The energy dependence of the various theoretical distributions may be compared to the data by normalizing the intensities at one energy. For the internal Compton effect from the K shell, the energy dependence of the calculations for the magnetic transition all show a consistent deviation from the data. In each case the theoretical distribution has a much smaller slope than the data. This effect may be significant in view of the fact that if the lack of intensity agreement was due to instrumentally produced background, the slope of the data would be smaller than the theoretical calculations. When the K and L shell contributions are considered together, the deviation of the energy distribution remains, although the agreement with the theories of Baumann and Robl, and Spruch and Goertzel is better. For the electric transition, the theoretical distributions for the K shell internal Compton effect are scattered around the data with Baumann and Robl's calculation predicting the best agreement.

As was stated in the introduction, one would hope that the internal Compton effect might provide another method of determining the multipole order of a transition. In order to check this possibility, calculations were performed on each theory for several values of multipolarity and the resulting curves compared to the data with respect to the intensity and energy distribution. An example of the distribution derived from Baumann and Robl's theory for the magnetic transition is illustrated in figure 17 and figure 18. It should be

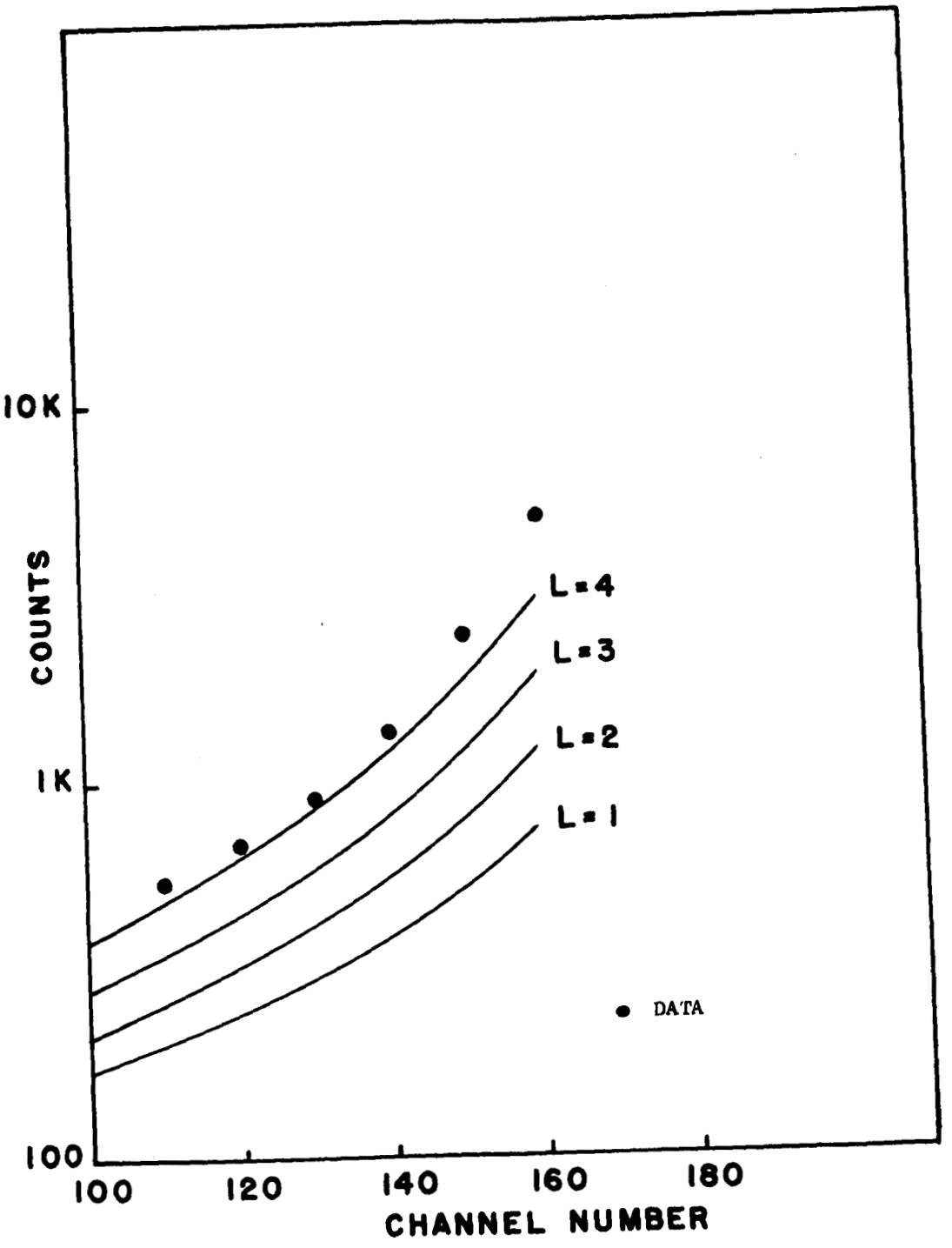

Fig. 17. Multipolarity dependence of Baumann and Robl's calculation where the internal conversion coefficient is known.

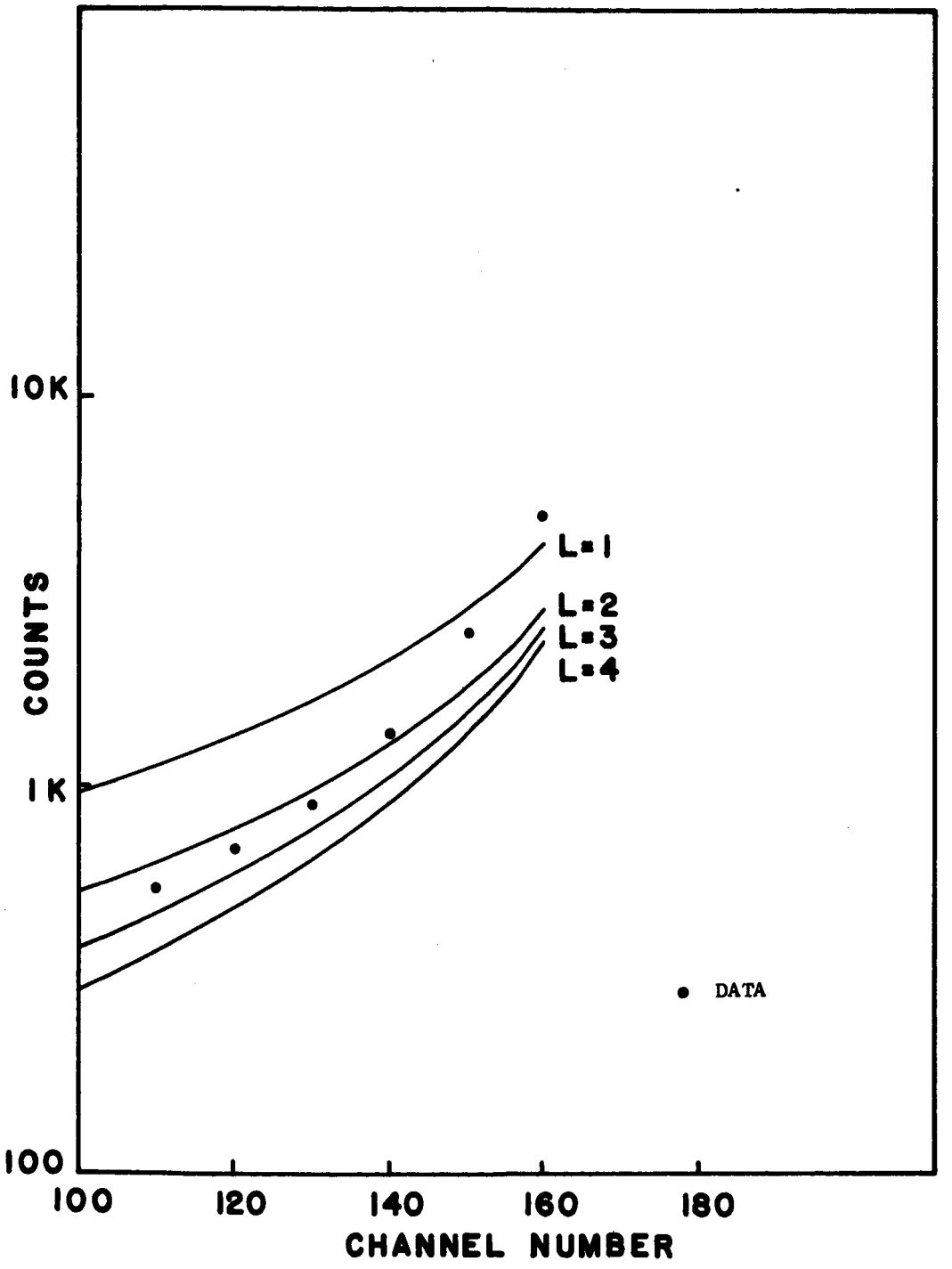

Fig. 18. Multipolarity dependence of Baumann and Robl's calculation where the internal conversion coefficient is taken from calculations in the Born approximation.

noted that where the α_K was assumed to be known, the intensity of the internal Compton effect increased with multipole order, while this dependence was reversed when the value of the conversion coefficient was taken from the Born approximation. The conclusions that can be derived from the comparison of the calculations to the observed data are listed in Table III where the experimental value of the internal conversion coefficient is used, and in Table IV where the coefficients are taken from the calculations in the Born approximation and are different for each multipolarity. It should be noted that the energy distribution was not a strong function of multipole order but at times could be used independently for a multipolarity assignment.

Another series of calculations were performed to ascertain whether the theoretical calculations were capable of distinguishing between the electric or magnetic character of a transition. This was done by applying the theoretical calculations for the electric transitions to the data resulting from the magnetic transition and conversely. The conclusions that were reached are listed in Table V. In general, the energy dependence of the distributions was in such poor agreement with the data that no multipolarity assignment could be made on this basis.

TABLE III

TRANSITION	AS PREDICTED BY BAUMANN AND ROBL (I)	(E)	IAKOBSON (I)
1064 keV, M4	N_K - M4	>M4	
570 keV, E2	N_K - E1	E1 or E2	N_K - E2

(I) Represents intensity comparison, (E) Represents energy distribution comparison.

TABLE IV

TRANSITION	SPRUCH AND GOERTZEL (I)	(E)	AS PREDICTED BY BAUMANN AND ROBL (I)	(E)	IAKOBSON (I)
1064 keV, M4	N_K - >M4	>M4	N_K - M2	N_K - >M4	
	N_{K+L} - >M4				
570 keV, E2			N_K - >E4	N_K - E2	N_K - <E1

(I) Represents intensity comparison, (E) Represents energy distribution comparison.

TABLE V

TRANSITION	SPRUCH AND GOERTZEL (I)	AS PREDICTED BY BAUMANN AND ROBL (I)	IAKOBSON (I)
1064 keV, M4		N_K - >E4 N_K - E3 α_K known	
570 keV, E2	N_K - M1		N_K - M1 N_K - M2-M3 α_K known

CHAPTER V

CONCLUSION

The purpose of comparing the theoretical predictions to the observed data is to identify the distributions below the conversion lines as resulting from the internal Compton effect. Although the agreement is not perfect, it is relatively certain that this is indeed a plausible explanation for the data.

There are however, certain reservations which must be considered. In applying the theoretical calculations to the distributions resulting from the decay of Bi^{207}, the requirements set by the Born approximation have been violated. The inequality $p>>\alpha Z$ indicated that the accuracy of the predictions should improve as the calculation approaches the energy of the conversion line. In this region, however, it becomes difficult to compare the theoretical distributions to the data because of the necessity to account for the distortion due to the resolution of the detectors.

As previously mentioned, the calculations of Baumann and Robl were applied in violation of the requirement $k>>\alpha Z$ which is only satisfied for small electron energies. Since the intensity of the internal Compton effect electron spectrum is peaked at high electron energies, it is difficult to satisfy this requirement and still have a measurable effect.

The Z dependence of the internal Compton effect coefficient illustrated in figure 19 indicates that it is a decreasing function of atomic number. This means that the probability of the internal Compton effect per conversion electron decreases with Z, but not necessarily the total intensity of the effect. Actually, the intensity increases with Z, but more slowly than the internal conversion coefficients. This fact indicates, that from the standpoint of intensity, it is worthwhile to study the high Z nuclei although currently available theoretical calculations are restrictive in this regard.

As indicated in figure 15, the contribution of the L shell internal Compton effect to that of the K shell is not negligible, and may significantly alter the intensity and the energy distribution. To provide an accurate comparison of the theoretical calculations to the data it is therefore necessary to consider the L shell contribution. As figure 15 illustrates, however, the calculations that were performed yielded little agreement, either among themselves or on the basis of comparison with the K shell calculations.

The agreement of the data and the theoretical predictions of the internal Compton effect, while sufficient to suggest the origin of the data, is not accurate enough to provide a unique determination of the character and multipolarity of the transitions in Bi^{207}. One of the possible advantages of making assignments on the basis of the internal Compton effect is that it has a distribution in energy that can be directly compared to the data. In many cases, the energy dependence of the internal Compton effect, while small, was more capable of distinguishing between multipole orders than was the intensity.

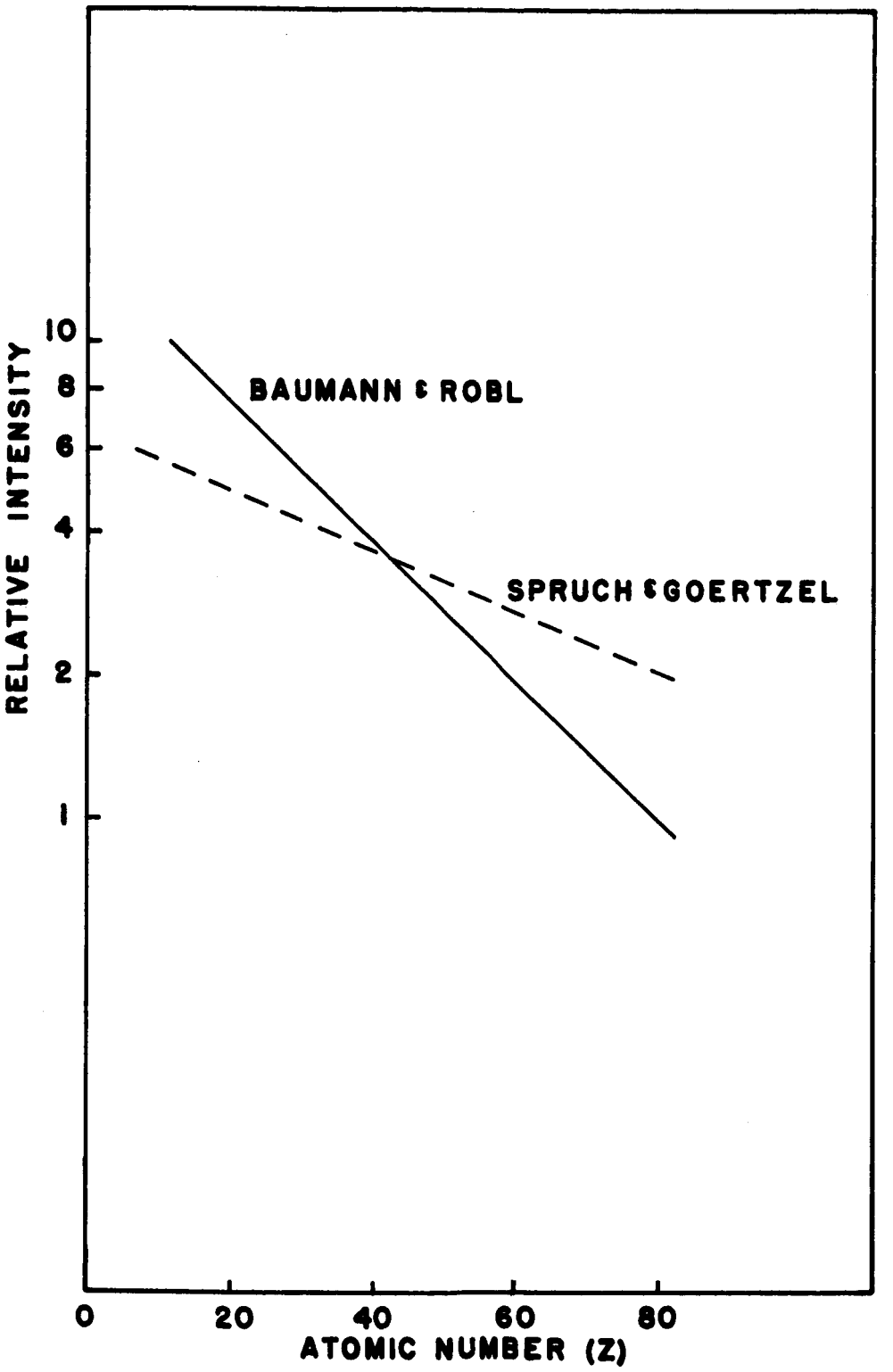

Fig. 19. The Z dependence of the internal Compton effect coefficient.

However, this requires that the energy dependence agree over some range in energy which is difficult to do when approximations favor one limit of the spectrum. The conclusion that can be reached on the determination of multipole orders and the character of the transition is that for a high Z nuclei such as Bi^{207}, the theoretical calculations yield inconsistent results.

LIST OF REFERENCES

1. H. M. Taylor and N. F. Mott, Proc. Roy. Soc. (London) 138A, 665 (1932); Proc. Roy. Soc. (London) 142A,215 (1933).

2. This discriptive term was suggested by C. H. Chen and J. Weinberg in a private communication.

3. H. B. Brown and R. Stump, Phys. Rev. 90, 1061 (1953).

4. E. Fuschini, C. Maroni, and P. Veronesi, Il Nuovo Cimento 26, 831 (1962).

5. E. Fuschini, C. Maroni, and P. Veronesi, Il Nuovo Cimento 41, 252 (1966).

6. T. Lindquist, B. Pettersson, and K. Siegbahn, Nuclear Physics 5, 47 (1958).

7. E. P. Cooper and P. Morrison, Phys. Rev. 57, 862 (1940).

8. W. J. Henderson, Proc. Roy. Soc. (London) 147A, 572 (1934).

9. J. K. Knipp and G. E. Uhlenbeck, Physica 3, 425 (1936).

10. C. S. Chang and D. L. Falkoff, Phys. Rev. 76, 365 (1949).

11. Von K. Baumann and H. Robl, Z. Naturforschg. 9a, 511 (1954).

12. A. M. Iakobson, Soviet Physics (JETP) 2, 751 (1956).

13. L. Spruch and G. Goertzel, Phys. Rev. 93, 642 (1954).

14. R. G. Fowler, Introduction to Electric Theory (Addison-Wesley Publishing Co. , Cambridge, Mass. , 1953), p. 175.

15. From table by L. A. Silv and I. M. Band, Alpha-, Beta- and Gamma Ray Spectroscopy Vol. 2 (North Holland Publishing Co. , Amsterdam, 1965), p. 1639.

16. J. W. Harpster, Thesis Western Reserve University Dept. of Physics, Physics 378.771, OH 2957.

17. D. E. Alburger and A. W. Sunyar, Phys. Rev. 99, 695 (1955).

"The aeronautical and space activities of the United States shall be conducted so as to contribute . . . to the expansion of human knowledge of phenomena in the atmosphere and space. The Administration shall provide for the widest practicable and appropriate dissemination of information concerning its activities and the results thereof."

—NATIONAL AERONAUTICS AND SPACE ACT OF 1958

NASA SCIENTIFIC AND TECHNICAL PUBLICATIONS

TECHNICAL REPORTS: Scientific and technical information considered important, complete, and a lasting contribution to existing knowledge.

TECHNICAL NOTES: Information less broad in scope but nevertheless of importance as a contribution to existing knowledge.

TECHNICAL MEMORANDUMS: Information receiving limited distribution because of preliminary data, security classification, or other reasons.

CONTRACTOR REPORTS: Technical information generated in connection with a NASA contract or grant and released under NASA auspices.

TECHNICAL TRANSLATIONS: Information published in a foreign language considered to merit NASA distribution in English.

TECHNICAL REPRINTS: Information derived from NASA activities and initially published in the form of journal articles.

SPECIAL PUBLICATIONS: Information derived from or of value to NASA activities but not necessarily reporting the results of individual NASA-programmed scientific efforts. Publications include conference proceedings, monographs, data compilations, handbooks, sourcebooks, and special bibliographies.

Details on the availability of these publications may be obtained from:

SCIENTIFIC AND TECHNICAL INFORMATION DIVISION

NATIONAL AERONAUTICS AND SPACE ADMINISTRATION

Washington, D.C. 20546